R. & M. No. 2863
(13,509, 13,789, 13,947)
A.R.C. Technical Report

MINISTRY OF SUPPLY

AERONAUTICAL RESEARCH COUNCIL
REPORTS AND MEMORANDA

Tests at High Subsonic Speeds on a 10 per cent Thick Pressure-plotting Aerofoil of RAE 104 Section

By
E. W. E. Rogers, D.I.C., B.Sc., C. J. Berry,
and
R. F. Cash, A.F.R.Ae.S.

LONDON: HER MAJESTY'S STATIONERY OFFICE
1956
THIRTEEN SHILLINGS NET

Tests at High Subsonic Speeds on a 10 per cent Thick Pressure-plotting Aerofoil of RAE 104 Section

By

E. W. E. Rogers, D.I.C., B.Sc., C. J. Berry, and R. F. Cash, A.F.R.Ae.S.,

of the Aerodynamics Division, N.P.L.

Reports and Memoranda No. 2863*

April, 1951

1. *Summary and Introduction.*—A series of tests has been made in the National Physical Laboratory 20-in. × 8-in. High Speed Wind Tunnel on a two-dimensional pressure-plotting aerofoil of five inches chord and RAE 104 section. The work included :

(*a*) A comparison of the results obtained with and without spanwise bulges on the aerofoil surface (Ref. 1).

(*b*) A comparison (to show the effects of a change in Reynolds number at high speeds) with measurements made in the same tunnel on a pressure-plotting aerofoil of similar profile but having a chord of two inches (Ref. 2).

(*c*) An investigation of the pressure distribution and flow around the aerofoil at high incidences for various Mach numbers.

(*d*) A determination of the force coefficients, surface pressures and flow patterns for the aerofoil through a range of Mach number at incidences up to 8 deg.

The present report is concerned with this last item.

2. *The Aerofoil.*—The five symmetrical aerofoils designed by Squire in 1945 and described by him in a note of limited circulation were originally referred to as ' Sections A to E '. Slightly different versions of aerofoils B, E and A were tested on a balance in the Royal Aircraft Establishment High Speed Tunnel and are called ' H.S. 6, 7 and 8 ' in the report[3] on that work. Subsequently however, the Squire sections were designated ' RAE 100 to 104 '. The ordinates and theoretical pressure distributions are given in Ref. 4.

RAE 104 (or Squire E) has a maximum thickness/chord ratio of 10 per cent occurring at 42 per cent chord. The rear section of the aerofoil beyond about 80 per cent of the chord is wedge shaped. At zero lift, the theoretical pressure distribution is almost constant back to 60 per cent chord and then falls uniformly to the trailing edge.

For the present tests the aerofoil was made with a finite trailing-edge thickness of 0·00064 chord and this modifies very slightly some of the ordinates given in Ref. 4. The actual model ordinates are given in Table 1 and the profile is shown in Fig. 1.

The model had seventeen pressure holes on the upper surface, fourteen on the lower surface, one at the leading edge and one at the trailing edge. Table 2 gives the chordwise positions of the pressure holes.

* Published with permission of the Director, National Physical Laboratory.

3. *Tests.*—(*a*) *Method of Testing.*—Using a large multi-tube manometer, measurements of the surface pressure distribution were made at various incidences from 0 deg to 8 deg for a Mach number range of from 0·4 to the limiting speed of the tunnel. The flexible walls of the tunnel were ' streamlined ' in the standard manner[5]. In addition, several pressure distributions were taken at negative incidences to check the symmetry of the flow and the accuracy of the zero incidence setting; these were satisfactory in all cases.

At the higher incidences, the model slightly affects the reading of the tunnel-speed hole 1·7 chords upstream of the leading edge and to allow for this a correction has been applied, where necessary, to the nominal free-stream Mach number.

Wake traverses were also made at one chord behind the trailing edge of the model for six incidences, the Mach number range being the same as for the pressure distributions.

The Reynolds number of the tests varied with Mach number between 1·1 and 1·9 million.

(*b*) *Reduction of the Observations.*—The coefficients C_L and C_m were found in the usual way by integrating the pressure distribution curves; the profile-drag coefficients (C_D) were obtained from the wake pitot-traverse curves by means of a shortened method of Ref. 6.

(*c*) *Flow Visualisation.*—Schlieren and direct-shadow photographs of the flow were obtained at most angles of incidence and free-stream Mach numbers. For the schlieren photographs, the cut-off was parallel to the aerofoil chord.

(*d*) *Condition of Boundary Layer.*—The tests were first made with the boundary-layer transition taking place naturally. Later the transition position was fixed on both surfaces at about 0·14 chord by means of a narrow band of cellulose lacquer (*see* section 7).

4. *Presentation of Results.*—The experimental pressure distributions obtained with the natural transition position are given in Figs. 3 to 15*; two methods of plotting these results are used:

(*a*) In terms of the pressure coefficient C_p $[= (p - p_0)/\frac{1}{2}\rho U^2]$.

(*b*) In terms of the ratio p/H for certain incidences.

(The stream total head and static pressure are denoted by H and p_0, and p is the measured surface pressure.)

A comparison with the theoretical pressure distributions at four angles of incidence for Mach numbers near 0·4 is made in Fig. 2.

The resulting lift and quarter-chord moment curves and their derivatives, together with the drag results are given in Figs. 17 to 30; a comparison with R.A.E. tests on a wing of aspect ratio 5·5 is also made (Figs. 32 to 34).

The results obtained with the boundary-layer transition artificially fixed at about 0·14 chord are presented in Figs. 35 to 43. Finally, direct-shadow and schlieren flow photographs for both conditions of the boundary layer are reproduced as Figs. 45 to 51.

5. *Discussion of Results (Transition Free).*—(*a*) $\alpha = 0$ *deg* (*Figs.* 3, 45 *and* 46).—Fig. 2 shows that at $M = 0{\cdot}4$ agreement between the calculated and experimental pressure distributions is reasonably good over most of the aerofoil surface. Between 0·6 and 0·7 chord there is a small discrepancy between the two curves, due to a kink in the experimental pressure distribution curve. This kink becomes accentuated with increase of Mach number (Fig. 3) and its position corresponds roughly with that of a local separation of the laminar boundary layer which was first detected by means of oil deposited on the model surface at a Mach number of 0·65. Transition occurs at about 0·75 chord, after reattachment of the boundary layer; the evidence of the direct-shadow photographs on this matter was subsequently confirmed by evaporation tests using α-monochlorhydrin as the indicator.

* Tabulated values of C_p or p/H for the various pressure distributions may be obtained on application to the Superintendent, Aerodynamics Division, N.P.L.

The experimental pressure-critical Mach number at zero incidence is 0·785, although Fig. 45c shows that small wavelets, presumably moving against the stream, are visible at $M = 0{\cdot}750$. No sudden change takes place in the flow pattern as the free-stream Mach number is raised above the critical, the diffuse band of wavelets slowly giving place to a series of shock-waves inclined forward into the stream. Each compression wave is followed by a small expansion, presumably as a result of undergoing reflection from the laminar boundary layer, which was found to be separated from the surface in this region. The number of these shock-waves decreases rapidly with increasing Mach number. For example, at $M = 0{\cdot}810$ (Fig. 46b) there are five or six separate waves visible between 0·4 chord and 0·7 chord; this is reduced to three or four inclined waves followed by a small normal wave in Fig. 46c ($M = 0{\cdot}820$), to one inclined wave followed by a normal wave at $M = 0{\cdot}840$ (Fig. 46e). It is between $M = 0{\cdot}800$ and $0{\cdot}820$ that the rapid increase in drag coefficient occurs; by $M = 0{\cdot}840$, C_D is twice its low-speed value and the loss of momentum through the shock-system has become appreciable. The value of C_p at the trailing edge also begins to decrease rapidly at this speed, indicating an increase in boundary-layer thickness at this position. (Separation of the turbulent boundary layer was not observed until about 0·88 (Fig. 16a).)

This change in the flow pattern modifies the shape of the pressure distribution curves until at $M = 0{\cdot}840$, there is the type of curve usually associated with a locally detached laminar layer upstream of the main shock-wave. These results are compared below with those obtained from the aerofoil with transition fixed on both surfaces at about 0·14 chord; in this case, there is no local separation of the boundary layer and the type of shock-pattern described above is absent. The local velocity continues to increase up to the final recompression and thus the 'truncated' type of pressure distribution is not observed.

As the free-stream Mach number is increased beyond 0·840, the pressure distribution curves remain similar in general shape, apart from the rearward movement of the recompression position. The flow photographs however show that the shock-pattern obtained at $M = 0{\cdot}840$ gives place to a normal shock-wave as the Mach number is raised to 0·860 (Figs. 45n and 46g). The laminar boundary layer separates upstream of the main wave and a weak compression wave springs from this point to join the main wave some distance from the aerofoil surface. Fig. 45n suggests that transition to turbulent flow in the separated, or vortex layer does not occur until just before the wave. Oil deposited on the model surface did not indicate any reversed flow in the turbulent boundary layer but the schlieren photograph (Fig. 46g) suggests that this layer may have been separated or about to separate.

The weak inclined compression waves* appear also in the schlieren photograph at $M = 0{\cdot}89$ (Fig. 46i). In this case there is a gradual compression immediately upstream of the foot of the main wave which now resembles a bifurcated wave[7], but with its front branch 'softened'. There is now definitely no attachment after transition to turbulent flow, the oil indicating reversed flow from the trailing edge to the foot of the shockwave for Mach numbers of 0·88 and above. The presence of turbulent separation is also suggested by Fig. 46i.

(*b*) $\alpha = 1$ *deg* (*Fig.* 4).—At this incidence the low-speed pressure distribution has a small suction peak on the upper surface near the leading edge. With increasing Mach number, the peak gradually disappears and the curve becomes similar in shape to that observed at the higher Mach numbers at zero incidence, with a favourable pressure gradient back to about 0·5 chord.

The lift coefficient increases continuously up to a Mach number of about 0·82, when sonic velocity is reached on the lower surface. The subsequent rapid growth in the local supersonic region on this surface and the associated decrease in pressure, are greater than the corresponding effects on the upper surface and as a result, the lift decreases.

* The weak compression waves are not very clear (at least near the surface) in the direct-shadow photographs (Figs. 45n, 45p, and 45q). This is probably due to the continuous nature of the compression and suggests that both types of pictures are necessary if a detailed knowledge of the flow around the aerofoil is required.

(*c*) $\alpha = 2$ *deg* (*Figs.* 5, 6, 47 *and* 48).—As was observed at $\alpha = 1$ deg, the low-speed pressure distribution (in good agreement with theory, *see* Fig. 2) gives place to a curve having a favourable pressure gradient back to about 0·5 chord, as the Mach number is increased. Further the fall-off in C_L again occurs just after sonic velocity has been reached on the lower surface ; the decrease in C_m takes place a little earlier, when the low-pressure supersonic region, originally situated at the nose, spreads beyond the quarter-chord position.

The flow photographs show a similar sequence of events to that observed at 0 deg, although this occurs at different Mach numbers on the two surfaces. A forward-inclined shock-wave reflecting as an expansion from the locally separated laminar boundary layer and followed by a normal shock gives place to a strong normal wave. The increased pressure rise at the foot of the shock causes marked boundary-layer thickening and leads to a very thick layer over the rear of the aerofoil and a rapid increase in drag. The trailing-edge pressure coefficient begins to decrease rapidly after $M = 0{\cdot}83$ (Fig. 16b). On the lower surface, Figs. 47d, 47e and 47f, show the reduction in the number of the forward-inclined waves with increasing Mach number.

(*d*) $\alpha = 2{\cdot}5$ *deg and* 3 *deg* (*Figs.* 7 *and* 8).—The chief difference between the results obtained at these incidences is in the shape of the C_L-curve near its peak (Fig. 17). This peak is marked at $\alpha = 2{\cdot}5$ deg, but is replaced at the higher incidence by a region of almost constant lift coefficient extending over a range of Mach number from 0·74 to 0·82. In both cases the fall in C_L takes place just after the speed of sound has been reached on the lower surface.

On the upper surface between $M = 0{\cdot}75$ and 0·80, the increasing region of low pressure caused by the rearward movement of the shock-wave is offset to some extent by the disappearance of the forward suction peak. The peak is higher, and the loss of lift resulting from its disappearance is greater, at 3 deg incidence than at $\alpha = 2{\cdot}5$ deg.

(*e*) $\alpha = 4$ *deg* (*Figs.* 9, 10 *and* 49).—Fig. 2 shows that agreement between the theoretical and experimental pressure distributions is not as good at $\alpha = 4$ deg than at the lower incidences, especially over the rear half of the aerofoil. Sonic velocity first occurs on the upper surface of the aerofoil, near the nose, at a Mach number of 0·550. The drag coefficient rises slowly as this speed is exceeded. As the shock-wave moves back, it takes with it the boundary-layer transition position and it is possible that the shallowness of the drag rise is due in part to the increased losses through the shock-wave being offset by the reduced skin friction. The local Mach number on the aerofoil surface ahead of the shock-wave is reasonably constant being between 1·3 and 1·4 for a wide range of Mach number (0·685 to 0·838). This is shown in Fig. 10a.

The fall in C_m once more occurs when the shock-wave moves back past the quarter-chord position. On the lower surface the pressure decreases more rapidly with increase in Mach number (Fig. 9b), than was the case at the lower incidence; this tends to reduce to some extent the rate at which the lift coefficient rises with increasing tunnel speed. The pressure-critical Mach number for the lower surface is about 0·80, corresponding approximately to the Mach number at which the lift coefficient begins to decrease.

At Mach numbers greater than about 0·75, the shape of the upper surface pressure distribution curves suggests that a local laminar separation takes place about 0·1 chord upstream of the normal shock-wave. (This separation was in fact confirmed by oil tests.) A small recompression occurs at this point and is visible as a faint black band, inclined to the stream direction, in the schlieren photographs. At the higher Mach numbers, there is a peculiar bulge in the upper-surface pressure distribution curve between 0·8 chord and 0·95 chord. A similar though less marked effect occurs at 3 deg incidence (Fig. 8a) and the phenomenon persists up to the highest test incidence. Increase in free-stream Mach number causes the bulge to disappear at some incidences, presumably when severe separation takes place over the rear of the aerofoil. It is difficult to account for this bulge; oil deposited on the surface at this position gave little direct evidence For example, at $\alpha = 4$ deg the bulge begins to be apparent in the pressure distribution

taken at $M = 0{\cdot}763$ and persists until $M = 0{\cdot}829$. An oil test* at about a Mach number of $0{\cdot}79$ indicated no local separation in this region, whilst at about $M = 0{\cdot}81$, the surface flow was reversed from the trailing edge to about $0{\cdot}6$ chord.

(*f*) $\alpha = 6$ *deg and* 7 *deg* (*Figs.* 11, 12 *and* 50; 13).—The flow around the aerofoil at 6 deg incidence is similar in many respects to that obtained at 4 deg. The drag coefficient begins to rise soon after the pressure-critical Mach number ($0{\cdot}430$) has been exceeded, the transition position moving back from the nose with the shock-wave. In the direct-shadow photograph taken at $M = 0{\cdot}594$ (Fig. 50a) small ' lambda ' waves are visible near the leading edge.

The bulges in the upper surface pressure distribution curves near the trailing edge are very marked at this incidence (Fig. 11a).

Three pressure distributions were taken at 7 deg in order to find the low-speed lift-curve slope in this region and also the low-speed drag coefficient. These pressure distributions are plotted in Fig. 13; the step in the curve near the nose suggests that the stall is beginning and in fact $dC_L/d\alpha$ does begin to decrease (*see* Fig. 18).

(*g*) $\alpha = 8$ *deg* (*Figs.* 14, 15 *and* 51).—Because of the high suction peak, and the ' stepped ' shape of the curve in this region, the pressure-critical Mach number is difficult to estimate. At low speeds the flow separates locally near the nose and reattaches as a thick turbulent layer. Fig. 51a shows that several small waves are visible in this region at $M = 0{\cdot}591$ and by $M = 0{\cdot}640$, a well-defined lambda shock has developed, the forward leg of which is caused by the separating boundary layer. It should perhaps be pointed out that a series of shock-waves which appear to be consecutive in a photograph, may in fact be distributed along the chord since the flow may not be entirely two-dimensional at high incidence. The schlieren photograph at $M = 0{\cdot}640$ (Fig. 51d) shows that the boundary layer has fully separated behind the shock-wave.

This is the Mach number at which the drag coefficient reaches a local maximum (Fig. 27), a reduction taking place until $M = 0{\cdot}680$. The laminar boundary layer adheres over the front part of the model (local laminar separation occurs at $0{\cdot}1$ chord at $M = 0{\cdot}665$ and about $0{\cdot}01$ chord at $M = 0{\cdot}60$), and thus the turbulent boundary layer is initially thinner and the subsequent turbulent separation less severe. A comparison of Figs. 51d and 51f shows a small decrease in the width of the wake. Moreover above $M = 0{\cdot}690$ the flow adheres around the nose and the pressure distribution curve becomes smooth back to the shock (Fig. 15a).

The beginning of the drop in C_D corresponds approximately to a marked rise in the lift coefficient, which reaches its peak at $M = 0{\cdot}74$. This rise, which was not observed at 6 deg incidence, seems to be due to a rapid backward movement of the shock-wave combined with the attainment of higher local Mach numbers at the nose of the aerofoil. By $M = 0{\cdot}765$, the shock-wave has only moved a little to the rear of its position at a Mach number of $0{\cdot}737$ (Figs. 14 and 15). Further, the velocity distribution up to the shock is similar in both cases (a local Mach number of about $1{\cdot}6$ being obtained at the nose) and hence the pressure coefficient in this region is increased. There is also a relatively large decrease in the lower-surface pressure coefficient, and the net result is a decrease in C_L. Fig. 15a shows that the bulge in the pressure distribution curve between $0{\cdot}8$ chord and $0{\cdot}95$ chord on the upper surface appears at the three highest test Mach numbers.

The variation with Mach number of the trailing-edge pressure coefficient at this incidence is given in Fig. 16f. Up to a Mach number of $0{\cdot}64$, the value of $C_{p\,\text{T.E.}}$ slowly decreases; beyond this Mach number the drag coefficient decreases, and there is a rapid increase of $C_{p\,\text{T.E.}}$. The initial decrease in $C_{p\,\text{T.E.}}$ corresponds to the thickening of the boundary layer and separation with Mach number. The rapid increase corresponds to the adherence of flow over the nose of the model, which causes a thinner boundary layer or wake at the trailing edge. The rise in C_L and decrease in drag coefficient is due directly to this effect. A further boundary-layer separation or thickening occurring at a Mach number of about $0{\cdot}7$ causes a reduction in $C_{p\,\text{T.E.}}$ and a final drag rise.

* The oil tests mentioned in this report were made by H. H. Pearcy during an investigation on the stalling characteristics of this aerofoil; except at 0 deg incidence the tunnel walls were not streamlined but were adjusted for uniform pressure along the empty tunnel. It is therefore difficult to relate precisely the Mach numbers of the two tests.

6. *Brief Discussion of Integrated Results (Transition Free).*—(*a*) *Lift.*—It is interesting to note in Fig. 17, at the lower incidences the agreement between the experimental rise of C_L with increasing Mach number and that predicted by the Glauert law. The falling-off in C_L is delayed until after the pressure critical Mach number has been exceeded, and is preceded by a marked peak in the curves for $\alpha = 1$ deg, 2 deg and 2·5 deg. At 3 deg however this sharp peak is replaced by a flat top extending over a considerable range of Mach number and as a result the lift-curve slope in this region alters appreciably.

At the higher angles of incidence no agreement can be expected with the Glauert law, because the pressure-critical Mach number is low. At $\alpha = 8$ deg, there is in fact, a large and rapid increase in C_L between $M = 0{\cdot}6$ and $0{\cdot}725$ probably due to the rearward movement of the shock-wave and of the position of flow separation (*see* above).

The C_L vs. α curve exhibits a change of slope in the region $\alpha = 0$ deg to 2 deg even at low speeds. Similar effects have been observed in earlier tests and can be attributed to the forward movement of the upper-surface transition point in this range; the value of $dC_L/d\alpha$ thus varies with incidence (*see* curves of Fig. 23). A further decrease in the lift-curve slope occurs at the highest incidence; in this case it is probably due to turbulent separation over the rear of the aerofoil.

(*b*) *Moment.*—Except at the lowest incidence, the increase in C_m with Mach number (Fig. 19) is everywhere greater than that predicted by the Glauert law and by Hilton's empirical formula[9]. The maximum value of C_m is, in general, quite well defined and occurs at progressively decreasing Mach numbers as the incidence increases.

The variation of C_m with incidence or lift coefficient is relatively small at low Mach numbers but becomes less so as the speed is increased.

(*c*) *Drag.*—At incidences of 2 deg and 4 deg (but not at 0 deg) the final rapid rise in drag is delayed until well beyond the pressure critical Mach number (Fig. 27). The drag rise is in fact delayed until approximately the ' crest critical Mach number ' is reached[19]. This is when sonic velocity is first achieved at the position where the aerofoil surface is tangential to the free-stream direction. At 4 deg there is a peculiar discontinuity in the curve near $M = 0{\cdot}80$, the drag coefficient actually reducing slightly as the Mach number increases. The effect was confirmed when the observations were repeated later. The wake-traverse curves suggest that this reduction is due to a decrease in the loss through the shock-wave (which is quite well developed) but the reason for such a decrease is not clear a present.

A similar type of curve but with a much more marked discontinuity was obtained at $\alpha = 8$ deg, a well-defined reduction in C_D occurring between $M = 0{\cdot}64$ and $0{\cdot}69$; this point was discussed in section 5 (*g*) above. Similar reductions in C_D occurring at the same incidence and about the same Mach number, have been observed in many American tests on 10 per cent thick symmetrical sections.

The theoretical profile-drag coefficient values[10] for different mean transition positions are also plotted in Fig. 27. Using the evidence[11] of the direct-shadow photographs transition for 0 deg was found to take place at about $0{\cdot}75$ chord at low speeds. The measured value of C_D was $0{\cdot}0048$ and this agrees well with theory if the latter is extrapolated to estimate transition position at $0{\cdot}75$ chord.

(*d*) *Comparison with R.A.E. Results.*—An early version of a 10 per cent RAE 104 aerofoil, having a rounded trailing edge* has been tested on a balance in the R.A.E. High Speed Tunnel[3] at a Reynolds number of one million. The model used was rectangular with an aspect ratio of 5·5 and for comparison the N.P.L. results have been reduced to the same aspect ratio by the method of Ref. 12.

* This early version (H.S.7) had almost the same trailing-edge angle as the present RAE 104 but was slightly thicker beyond about 0·5 chord for a given x/c position. The trailing-edge thickness was reduced to zero by rounding the wedge tail after 0·975 chord. Until recently the RAE 104 section was known at the N.P.L. as H.S.7a.

It appears from Fig. 32, which compares the C_L vs. α curves, that although agreement is good at a Mach number of 0·4, the lift-curve slope of the N.P.L. results is less than that given by the R.A.E. tests at the higher Mach numbers. Reasonably good agreement in the curves of C_m against C_L is obtained for the two sets of results (Fig. 33), with the exception of near the stall at $M = 0{\cdot}4$. Here the divergence may be due to the different nature of the stall in the two cases of finite and infinite aspect ratio.

The drag results from the R.A.E. tests are not given in Ref. 3, but are included in a later paper. A comparison between the C_D vs. Mach number curves is given in Fig. 34, the N.P.L. results having been reduced to an aspect ratio of 5·5. The differences between the two sets of curves may be due partly to the effect of Reynolds number and partly to uncertainty in allowing for the effect of aspect ratio, particularly at the higher Mach numbers. Moreover, the R.A.E. wing had square-cut ends (the usual rounding of the section being omitted in this case) and it is understood that there was some uncertainty regarding the strut interference corrections to drag coefficient at high speeds.

7. *Tests with Fixed Boundary-Layer Transition Position.*—In the tests considered above, the boundary-layer transition was allowed to occur naturally and thus the layer was laminar up to the foot of the shock-wave system, when this was present on the aerofoil surface. At the rather low Reynolds numbers of the experiment (1·1 to 1·9 million), local separations of the laminar boundary layer tended to occur at some incidences and Mach numbers, giving rise to a characteristic type of shock-pattern and pressure distribution. Since the extent and magnitude of these operations (and their effect on the aerofoil surface pressures and forces) is known to vary with Reynolds number[2, 13], becoming less pronounced as this quantity is increased, results obtained with a natural transition position are difficult to extrapolate to a higher Reynolds number. Should the transition occur near the nose, so that the boundary layer ahead of the shock-wave is turbulent, then the present 'transition free' results may actually be misleading.

It was therefore felt that if transition could be fixed near the leading edge on both surfaces, a comparison of the results thus obtained with the earlier tests would be of interest.

Earlier experiments in the 20-in. × 8-in. Tunnel in which the boundary-layer transition position was fixed on an aerofoil were made by Pearcey[14]*, Shaw[15], and Fage and Sargent[16]. In the tests described in Ref. 14, spanwise wires were attached to the model in order to cause transition. It was concluded that for an aerofoil of 5-in. chord, this method was rather unsuitable due to the formation of shock-waves at the wires for comparatively low free-stream Mach numbers. By using a one-foot chord model (thus increasing the Reynolds number) the compressibility effects at the wires were found to be of less importance†. This model size however is too large for normal experimental work in the 20-in. × 8-in. Tunnel.

For the results obtained in Ref. 15, tests were made with the aerofoil in the wake of a fine wire (0·025-in. diameter) stretched across the tunnel 0·75 aerofoil chords upstream of the model and parallel to its leading edge; turbulent boundary layers were therefore caused on both surfaces of the aerofoil. The main objections to such a technique are:

(*a*) The drag of the model is difficult to measure by the wake-traverse method (the tunnel has no balance).

(*b*) The aerofoil is tested in a narrow non-uniform stream (the wake of the wire) whose mean Mach number is lower than that of the free stream.

(*c*) The flow just outside the boundary layer is more turbulent than would normally be the case had transition taken place at the leading edge in the absence of the wire. This may cause a more rapid growth in the boundary-layer thickness than would occur naturally.

---

* Pearcey has also made extensive tests on an aerofoil with turbulent and laminar boundary layers. These results are as yet unpublished.

† It was also found from tests in another tunnel of the N.P.L. High Speed Laboratory that spanwise grooves were ineffective in fixing transition on a 2-in. chord model.

Nevertheless, the results obtained from tests of this type are valuable in indicating the nature of the flow changes that occur when the boundary layer of the model is made turbulent at the leading edge. The effect of items (*b*) and (*c*) on the general flow pattern and the surface pressure distribution is difficult to assess and may well prove to be negligible.

Fage and Sargent[16] achieved a satisfactory method of causing transition by injecting air into the boundary layer at the required position through a spanwise row of small holes in the surface of a hollow aerofoil. By controlling the airflow, transition could be made to take place without disturbing the external flow. The method requires a specially constructed model and a chordwise variation of the transition position on a particular aerofoil is difficult. Moreover, on a 5-in. chord pressure-plotting model, these transition holes are normally only obtained by slightly reducing the number of chordwise pressure holes. The construction of a model of this design is not easy and its use in the wind tunnel may entail certain experimental difficulties.

It was therefore considered worthwhile attempting to fix transition by means of the method described below, which uses a narrow band of cellulose lacquer deposited near the leading edge to disturb the boundary layer.

(i) *Experimental Details and Range of Tests.*—Two spanwise parallel strips of cellulose tape were placed on the aerofoil surface with their edges about 0·03 chord apart and a thin coat (about 0·0015-in. thick) of Frigilene* applied over the inner edges of the strips and the surface between them. When this first application was dry, the process was repeated, the numbers of separate coats varying between two and five and depending on the chordwise position of the tapes and the free-stream Mach number of the tests (*see* below).

With the removal of the tapes a band of Frigilene was left which had sharply defined edges. It was found that, in general, a sharp forward edge to the band was essential for causing transition. When this edge became smoothed (for example, after several tunnel runs), the band was no longer effective.

Transition was fixed in this way on both surfaces of the aerofoil at a mean position of 0·14 chord. During the subsequent tests, the free-stream Mach number was varied between 0·4 and its limiting value for three values of incidence, 0 deg, 2 deg and 4 deg. Pressure distributions (Figs. 35 to 37) were recorded in order to determine C_L and C_M (Fig. 38), the drag coefficient (Fig. 39) being found by integrating the curves of total-head loss in the wake, one chord behind the trailing edge. In addition schlieren and direct-shadow photographs were taken of the flow around the model.

At free-stream Mach numbers where the local flow at 0·14 chord is supersonic, it proved difficult, though not impossible, to obtain a band of sufficient thickness to cause transition but not to produce small shock-waves at the band position. It was decided not to attempt to eliminate the waves completely but to reduce their magnitude and extent. Those visible in the photographs do not seem to affect appreciably the general flow, and in no case could an irregularity be detected in the readings of the neighbouring pressure holes. The addition of carborundum powder to the Frigilene, although causing transition even when the sharp forward edge of the band had worn away, greatly increased the size of the waves and this method was not used to obtain any of the results presented in the present note.

Tests were also made at two Mach numbers (0·4 and 0·725) for zero incidence, the profile drag being measured for various chordwise transition positions. The results obtained are compared with theory in Fig. 44.

At 0 deg incidence, for a given chordwise position, a thicker band was needed to cause transition at the lower speeds (and hence lower Reynolds number) than at the higher free-stream velocities, the pressure gradient being favourable back to at least 0·5 chord for all Mach numbers. The disturbance required to promote transition increased as the band position was moved to the rear of the model.

* A proprietary brand of cellulose lacquer.

At incidences of 2 deg and 4 deg and without a transition band, transition occurs near the nose on the upper surface at low speeds ; as the main shock-wave moves back with increasing free-stream Mach number, it carries the transition point with it. In this case then, a transition band situated at 0·14 chord would only begin to be effective after the local velocity at that point was supersonic. The thickness required at any particular free-stream Mach number was about the same as at 0 deg. On the lower surface, transition occurs well towards the rear of the aerofoil if no band is present. The band thickness necessary to cause transition at 0·14 chord on this surface was greater at low speeds.

The effectiveness of the band in provoking transition along the whole span of the model was checked at frequent intervals throughout the experiment by observing the evaporation of a thin film of glycerol-α-monochlorhydrin[11]. A well-defined transition front at the Frigilene band was always obtained. (The same chemical, applied more thickly so that its *movement* could be observed was also used in the earlier tests to detect local separations of the laminar boundary layer.) Similar observations made when transition was fixed at 0·14 chord failed to reveal any separation of the turbulent layer, except at the highest Mach number, where the oil flow on the aerofoil surface was reversed in direction from the trailing edge to about 0·8 chord.

(ii) *Discussion of Results—Transition Band at* 0·14 *Chord.*—It has been suggested by H. H. Pearcey that at relatively low Reynolds numbers, the differences in the general flow pattern when the boundary layer is either laminar or turbulent are due very largely to the presence of extensive local separations in the former case, which are absent when the boundary layer is turbulent. Such differences are much less noticeable when the laminar separations are smaller in extent and this occurs when the Reynolds number or the free-stream turbulence is increased (*see,* for example, Refs. 2 and 13).

It is proposed here merely to present the data obtained during the tests described above and to discuss the results briefly. The free-stream turbulence was low, and the test Reynolds number was also comparatively small (1·1 to 1·9 million).

(*a*) $\alpha = 0$ *deg* (*Figs.* 35, 45 *and* 46).—The pressure distribution curves obtained with either fixed or ' natural ' transition positions are shown in Figs. 35a to 35j ; specimen photographs of the flow pattern are given in Figs. 45 and 46.

At low speeds, the chief difference in the pressure-distribution curves occurs in the region between 0·6 chord and the trailing edge, the distribution with fixed transition position being in better agreement with theory[4] (Fig. 41). Above $M = 0{\cdot}6$, a local laminar separation was observed in the original tests between about 0·6 chord and 0·7 chord by means of α-monochlorhydrin deposited on the aerofoil surface.

From $M = 0{\cdot}820$ to 0·880, the pressure distributions obtained with a laminar boundary layer have the characteristic truncated appearance associated with a local separation ahead of the shock-wave system. With a turbulent boundary layer no such separation occurs and the main recompression on the aerofoil surface takes place more abruptly (*e.g.*, Figs. 35h to 35j). The main recompression systems in the two cases are situated at approximately the same chordwise position (Fig. 42a).

The shock-patterns in this Mach number range are dissimilar. For example at $M = 0{\cdot}820$, as was mentioned above, with a laminar boundary layer, there is a series of small compression waves, inclined upstream slightly, and each reflecting as an expansion from the separated layer (Fig. 46c), whilst with a turbulent boundary layer (Fig. 46d), the main compression wave is quite well-defined, normal to the surface and followed by a fairly rapid thickening of the boundary layer. In both cases the drag coefficient at this Mach number has increased by about the same amount above the value at $M = 0{\cdot}4$ (*see* Fig. 40).

Perhaps the most striking difference between the shock-patterns occurs at $M = 0{\cdot}840$ (Figs. 46e and 46f). In the original tests, the compression system consists of a forward-inclined wave reflecting as an expansion from the detached laminar layer, subsonic flow being finally reached

through a small normal shock ; the boundary layer reattaches to the surface in a turbulent state. When transition is made to occur at 0·14 chord, the main shock-wave is inclined downstream slightly at the surface, and becomes normal to the incident flow some distance from the aerofoil. This pattern is again observed at $M = 0{\cdot}860$ (Fig. 46h) but the backward inclination of the shock-wave near the surface is more marked. With a laminar boundary layer, the main compression wave has straightened and grown in extent ; the expansion region has disappeared, but separation still occurs some distance ahead of the main wave, giving rise to weak inclined compression waves and a softening at the foot of the main wave.

For the highest test Mach number at this incidence ($M = 0{\cdot}880$), the main compression waves are situated at about the same chordwise position in both tests, and are both inclined backwards near the aerofoil surface. The laminar boundary layer separates about 0·2 chord upstream of the main shock, causing (as before) weak inclined waves. These compression waves cause a small decrease in the local Mach number at that position (Fig. 35j). With a turbulent boundary layer, separation only takes place after the shock, the local Mach number increasing continuously up to the foot of the shock-wave.

(*b*) $\alpha = 2$ *deg* (*Figs.* 36 *and* 48).—At the lower speeds, the main difference between the two sets of pressure distribution curves at this incidence is the small increase in lower surface pressures when the boundary layer is turbulent from 0·14 chord. This discrepancy is greatest over the last 0·4 chord and in some cases (*e.g.*, Figs. 36c, 36d and 36*e*) the negative pressure-loop observed with a laminar boundary layer completely disappears. As a result, the lift coefficient is increased and the quarter-chord pitching-moment coefficient reduced (Fig. 38). On the upper surface the boundary layer is turbulent from near the nose in both cases and agreement is good over most of the surface.

The pressure-critical Mach number at $\alpha = 2$ deg is 0·720 but the flow patterns are similar up to about $M = 0{\cdot}770$; apart from small waves caused by transition band, only diffuse wavelets can be seen. By about $M = 0{\cdot}80$ the main shock-wave has become well-defined when the boundary layer is turbulent and the state of the boundary layer upstream of the shock-wave position is now important in determining the flow pattern and pressure distribution. Near $M = 0{\cdot}82$, for example (Figs. 48e and 48f), the shock-waves on the upper surface and the associated pressure distributions differ in a similar manner to that observed at 0 deg. The continuous decrease in pressure back to the shock-wave, which occurs with a turbulent boundary layer, causes an increase in the lift coefficient (Fig. 38).

On the lower surface where the local velocity at about 0·55 chord is just supersonic at this Mach number, the pressure distribution curves in this region are in each case similar in type to those observed on the upper surface around 0·5 chord (Fig. 36g).

The pressure-distribution curves at $M = 0{\cdot}840$ and 0·841 (Fig. 36h) illustrate well the characteristic difference in shape obtained with the two states of the boundary layer.

The increase in drag coefficient above the value obtained at $M = 0{\cdot}4$ is slightly greater with a turbulent boundary layer at Mach numbers above 0·75. The final drag rise occurs earlier, the difference in free-stream Mach number being about 0·02 (Fig. 40).

(*c*) $\alpha = 4$ *deg* (*Figs.* 37 *and* 49).—In general, the differences between the two sets of results at this incidence are similar to those observed at $\alpha = 2$ deg. At all speeds, the lift coefficient is higher when transition is fixed on both surfaces. At low Mach numbers, this is due to small changes in C_p, particularly on the lower surface. For higher free-stream Mach numbers, this effect is augmented by the lower pressure just upstream of the main shock-wave when the boundary layer is turbulent and the change in the pressure distribution to the rear of this position. The bulge in the upper surface pressure distribution between 0·8 and 0·9 chord observed with a laminar boundary layer ahead of the shock, disappears when transition is fixed at 0·14 chord (*see* Figs. 37f and 37g).

Between about 0·15 and 0·45 chord, the upper surface of the aerofoil is obscured by the holes in the glass tunnel wall, through which pass the model support pins. A comparison of the bases of the shock-waves and their interaction with the aerofoil boundary layer in the two cases, is

difficult until about $M = 0{\cdot}77$. Figs 49e and 49f show that with a laminar boundary layer the main compression wave is inclined forward slightly into the stream ; with transition fixed at $0{\cdot}14$ chord, the shock-wave is inclined slightly downstream near the surface. The corresponding pressure distributions (Fig. 37e) suggest that a local laminar separation takes place at about $0{\cdot}15$ chord upstream of the main shock-wave in the former case.

Near $M = 0{\cdot}80$, the flow behind the shock-wave system is different in the two tests, a more rapid thickening of the boundary layer occurring with a fixed transition position. Some thickening of the boundary layer also occurs ahead of the shock in this case giving rise to a region of continuous compression. This region grows in extent as the free-stream Mach number is increased. When the boundary layer is laminar upstream of the shock-wave, this continuous compression still exists (*cf.* Figs. 37g and 37h), although it is more gradual and is spread over a larger fraction of the chord. It begins at the forward limit of the local laminar separation and a faint compression wave originating from this point can just be seen in Figs. 49i and 49k.

The drag rise occurs earlier and the subsequent rate of increase of C_D with M appears to be greater when transition is fixed (Fig. 43).

(*c*) *Discussion of Results—Transition Band at Various Chordwise Positions.*—The variation of measured C_D with Mach number at zero incidence is plotted in Fig. 43 for the two cases of ' natural ' and ' fixed ' transition positions. The theoretical values[10] of C_D for various transition positions are also given and it is seen that these predict a position nearer the trailing edge than was actually the case. The discrepancy is greater at the lower Mach numbers.

Transition was therefore fixed by means of a Frigilene band at five additional chordwise stations at a free-stream Mach number of $0{\cdot}4$ and the profile-drag coefficient measured. A linear reduction of C_D with rearward movement of transition position was observed (Fig. 44a). The corresponding theoretical curve gives everywhere a higher value of C_D for a given transition position, the difference between the two lines reducing with rearward movement of the band. Similar curves were obtained at $M = 0{\cdot}725$, but only one additional transition position was investigated (Fig. 44b).

A difference of the same order between the experimental and theoretical results has been observed earlier by Dowlen[17] (wind-tunnel tests) and R. C. Lock[18] (flight tests). The latter report discusses the matter at some length without reaching any definite conclusions. Dowlen attributes the discrepancy to the fact that at the low Reynolds number of his tests ($1{\cdot}1 \times 10^6$), transition took place over an appreciable chordwise region (about $0{\cdot}2$ chord) and was not immediately provoked by the disturbing wire. In the tests described in the present note (which are at the same Reynolds number as Dowlen's at $M = 0{\cdot}4$), a sharp well-defined transition front was given by the indicator and it is considered unlikely that transition could extend over about $0{\cdot}15$ chord—the requisite chordwise distance at $M = 0{\cdot}4$.

8. *Concluding Remarks.*—These tests made in the 20-in. × 8-in. High Speed Wind Tunnel with a 10 per cent thick RAE 104 aerofoil, in addition to providing data on the behaviour of the section for a range of Mach numbers and incidence, show that large differences in flow pattern, pressure distribution and force coefficients can be obtained by fixing boundary-layer transition near the nose on both surfaces. These changes are mainly due to the suppression (or at least, reduction in chordwise extent) of the local boundary-layer separations observed near the feet of the shock-waves in the original tests[2].

There is evidence to suggest that the influence of these local laminar separations on the aerodynamic characteristics of an aerofoil decreases with increase of Reynolds number, even though the boundary layer remains laminar up to the shock-wave system. Tests planned in the new pressurised 18-in. × 14-in. Tunnel (R up to 6 million) on a 5-in. chord pressure-plotting aerofoil of the same section and thickness/chord ratio as the present tests, will therefore be of interest.

The Frigilene-band technique described in this report, though easy to apply, requires constant vigilance on the part of the tunnel operators as the band tends to become ineffective after a little time. Small shock-waves are difficult to eliminate and the band thickness necessary to cause transition varies with Mach number (linked with Reynolds number in the 20-in. × 8-in. Tunnel) and chordwise position of the band.

The method therefore, can be said to be useful when various transition positions are required or when only a limited amount of work with a fixed transition position is contemplated. For routine tests in which transition position remains constant and in which careful control of the disturbance is necessary, the introduction of air into the boundary layer through small surface holes would seem to be best*. More definite conclusions will be possible after the tests on the 6 per cent RAE 104 aerofoil have been completed.

9. *Acknowledgement.*—The authors wish to acknowledge the assistance given by Miss B. M. Davis both during the experimental work and in the preparation of the figures and photographs.

REFERENCES

No.	*Author*	*Title, etc.*
1.	J. A. Beavan, E. W. E. Rogers and R. Cartwright.	High Speed Wind Tunnel tests on an aerofoil with and without two-dimensional bulges. C.P.78. February, 1951.
2.	E. W. E. Rogers, A. Chinneck and R. F. Cash.	A comparison of results obtained at high subsonic speeds on two aerofoils of similar section but differing chord. A.R.C. 13,628. December, 1950. (Unpublished.)
3.	R. Hills and H. E. Gamble ..	Preliminary note on three 10 per cent thick aerofoils (H.S.6, 7, 8) in the R.A.E. High Speed Tunnel. R.A.E. Tech. Note Aero. 1926. A.R.C. 11,117. December, 1947. (Unpublished.)
4.	R. C. Pankhurst and H. B. Squire..	Calculated pressure distributions for the RAE 100–104 aerofoil sections. C.P.80. March, 1950.
5.	C. N. H. Lock and J. A. Beavan ..	Tunnel interference at compressibility speeds using the flexible walls of the Rectangular High Speed Tunnel. R. & M. 2005. September, 1944.
6.	J. A. Beavan and A. R. Manwell ..	Tables for use in the determination of profile drag at high speeds by the pitot traverse method. R. & M. 2233. September, 1941.
7.	A. Fage and R. F. Sargent ..	Shock wave and boundary layer phenomena near a flat surface. *Proc. Roy. Soc.* A, Vol. 190. 1947.
8.	E. W. E. Rogers and C. White ..	Force and pressure measurements up to Mach number 0·88 on a 10 per cent thick modified NACA 16 series propeller section A.R.C. 11,114. 24th December, 1947. (Unpublished.)
9.	W. F. Hilton	Empirical laws for the effect of compressibility on quarter-chord moment coefficient, and for the choice of an aerofoil with small compressibility effects on centre of pressure. R. & M. 2195. March, 1943.
10.	N. E. Winterbottom and H. B. Squire.	Note on further wing profile drag calculations. R.A.E. Report B.A.1634. A.R.C. 4781. October, 1940.
11.	H. H. Pearcey	The indication of boundary layer transition on aerofoils in the N.P.L. 20-in. × 8-in. High Speed Wind Tunnel. C.P.10. December, 1948.
12.	A. D. Young	Note on the effect of compressibility on the lift curve slope of a wing of finite span. R. & M. 2767. August, 1943.
13.	R. Hills	Use of wind tunnel model data in aerodynamic design. *J.R. Ae. Soc.*, Vol. 55, pp. 1 to 19. January, 1951.
14.	H. H. Pearcey	Aerofoils with and without spanwise wires or grooves. R. & M. 2252. August, 1942.
15.	R. A. Shaw	Adhesion of flow beyond the shock stall on an E.C.1250 aerofoil with 25 per cent concave control flap. Further tests with turbulent boundary layer. R. & M. 2436. April, 1949.
16.	A. Fage and R. F. Sargent ..	An air-injection method of fixing transition from laminar to turbulent flow in a boundary layer. R. & M. 2106. June, 1944.

* Subsequent experiments have confirmed this view.

REFERENCES—*continued*

No.	*Author*	*Title, etc.*
17.	E. M. Dowlen	A comparison of the calculated profile drag coefficients of various low-drag wing sections. College of Aeronautics Report No. 35. A.R.C. 13,224. April, 1950.
18.	R. C. Lock	Note on profile drag calculations for low-drag wings with cusped trailing edges. R. & M. 2419. April, 1946.
19.	R. F. Cash	Application of suggested drag-rise criterion to some N.P.L. and D.V.L. drag measurements on two-dimensional aerofoils at high subsonic Mach numbers. A.R.C. 13,689. January, 1951. (Unpublished.)

TABLE 1

Ordinates of RAE 104

x/c	*y/c*	*x/c*	*y/c*	*x/c*	*y/c*
0	0	0·10	0·03234	0·58	0·04590
0·001	0·00344	0·12	0·03498	0·60	0·04464
0·002	0·00486	0·14	0·03724	0·62	0·04310
0·003	0·00596	0·16	0·03924	0·64	0·04136
0·004	0·00688	0·18	0·04100	0·66	0·03948
0·005	0·00768	0·20	0·04256	0·68	0·03746
0·006	0·00840	0·22	0·04394	0·70	0·03534
0·007	0·00908	0·24	0·04516	0·72	0·03312
0·008	0·00970	0·26	0·04622	0·74	0·03086
0·010	0·01082	0·28	0·04714	0·76	0·02854
0·012	0·01184	0·30	0·04790	0·78	0·02620
0·014	0·01276	0·32	0·04856	0·80	0·02382
0·016	0·01364	0·34	0·04908	0·82	0·02148
0·018	0·01446	0·36	0·04948	0·84	0·01912
0·020	0·01520	0·38	0·04976	0·86	0·01678
0·025	0·01696	0·40	0·04994	0·88	0·01442
0·030	0·01852	0·42	0·05000	0·90	0·01208
0·035	0·01994	0·44	0·04994	0·92	0·00972
0·040	0·02126	0·46	0·04976	0·94	0·00738
0·050	0·02362	0·48	0·04944	0·96	0·00502
0·060	0·02568	0·50	0·04902	0·98	0·00268
0·070	0·02756	0·52	0·04846	1·00	0·00032
0·080	0·02928	0·54	0·04776		
0·090	0·03086	0·56	0·04692		

TABLE 2

Position of Pressure Holes

Hole No.	*x/c*		Hole No.	*x/c*	
	Upper	Lower		Upper	Lower
L.E.	0	0	10	0·50	0·62
1	0·002	0·005	11	0·56	0·68
2	0·01	0·02	12	0·62	0·74
3	0·04	0·10	13	0·68	0·83
4	0·10	0·16	14	0·74	0·95
5	0·16	0·26	15	0·80	
6	0·26	0·36	16	0·88	
7	0·30	0·44	17	0·95	
8	0·36	0·50	T.E.	1·00	1·00
9	0·44	0·56			

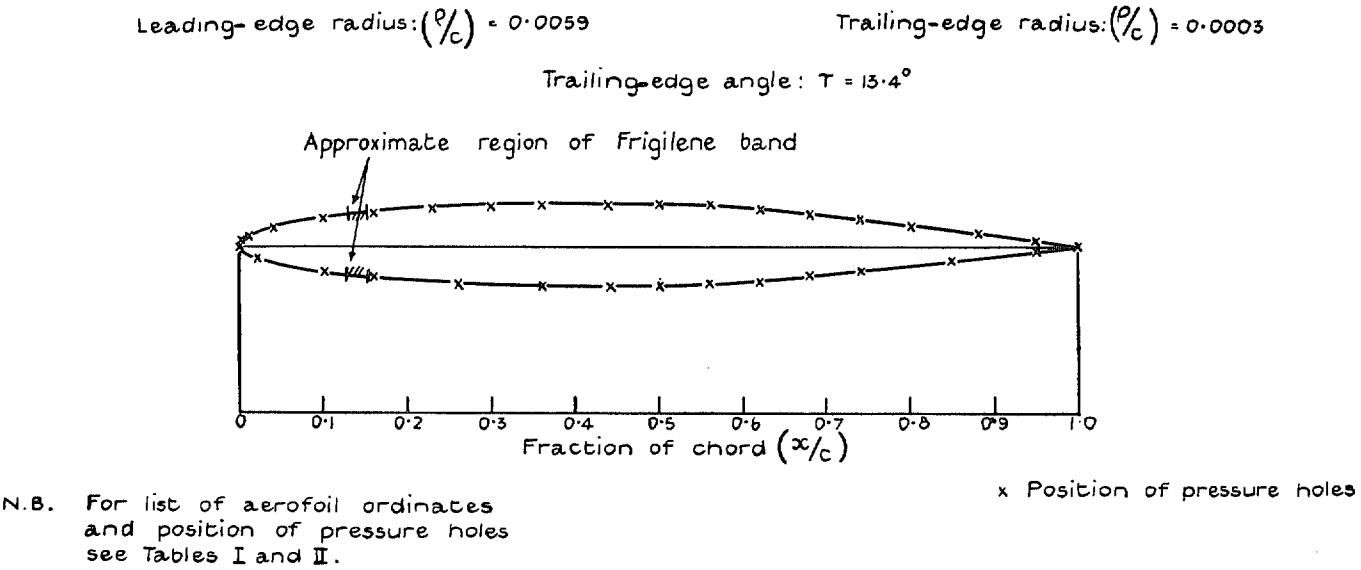

FIG. 1. RAE 104 aerofoil, 5-in. chord.

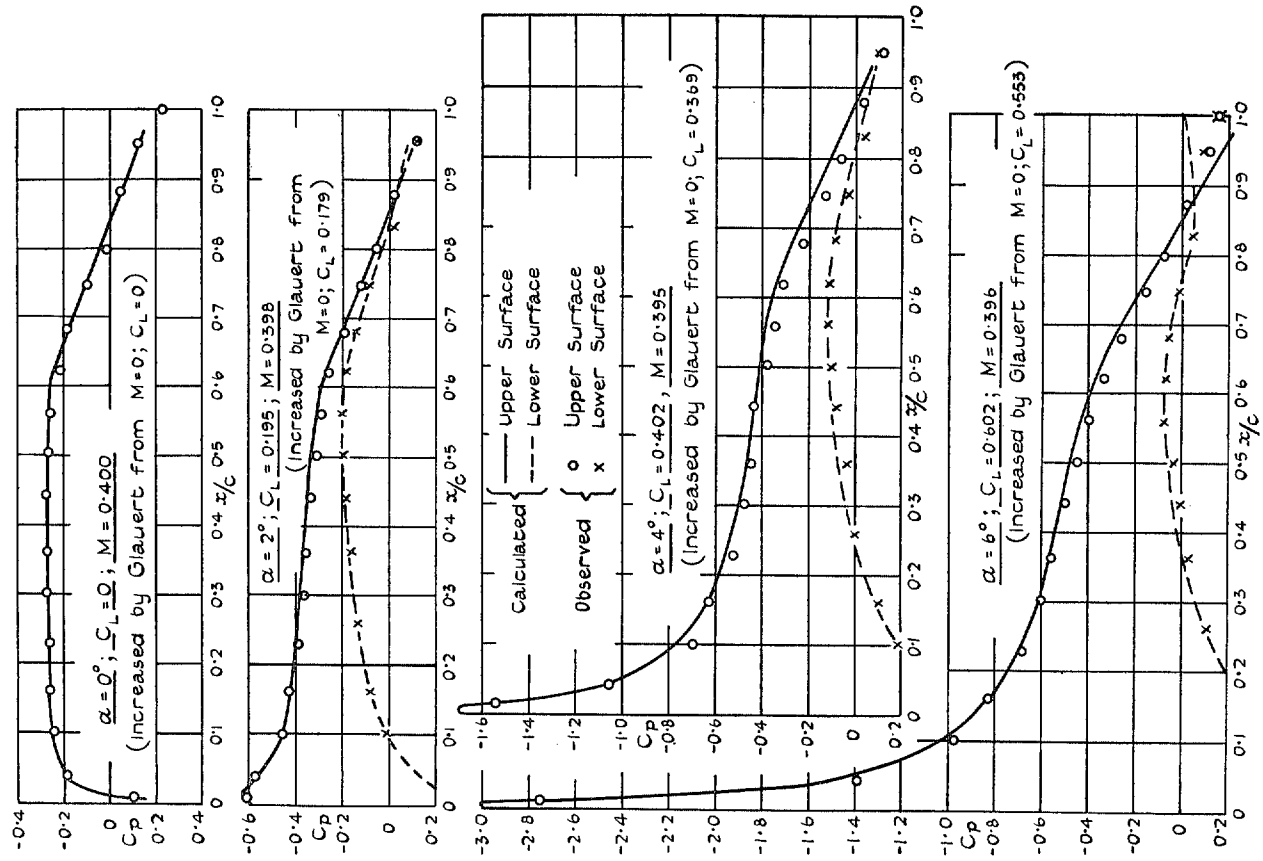

FIG. 2. Comparison of calculated and observed pressure distributions.

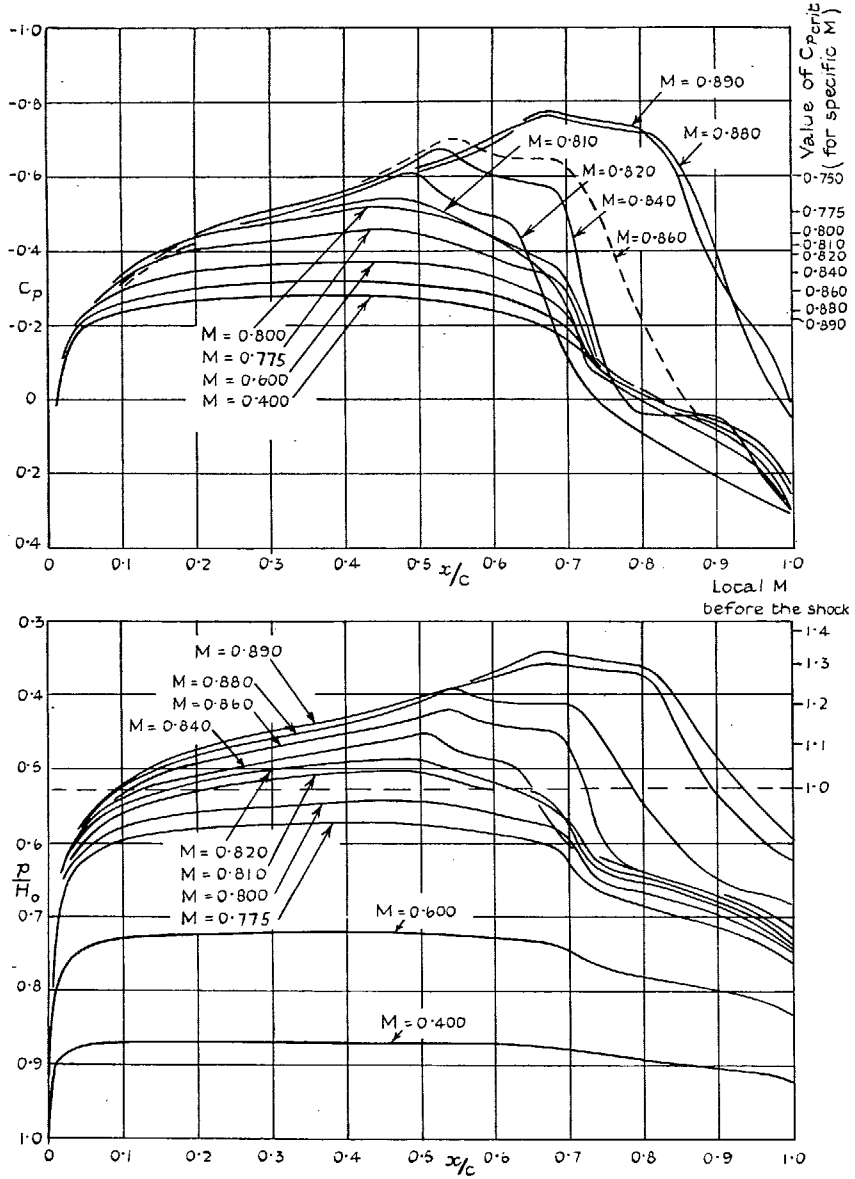

FIG. 3. 10 per cent RAE 104 aerofoil : pressure distributions at $\alpha = 0$ deg.

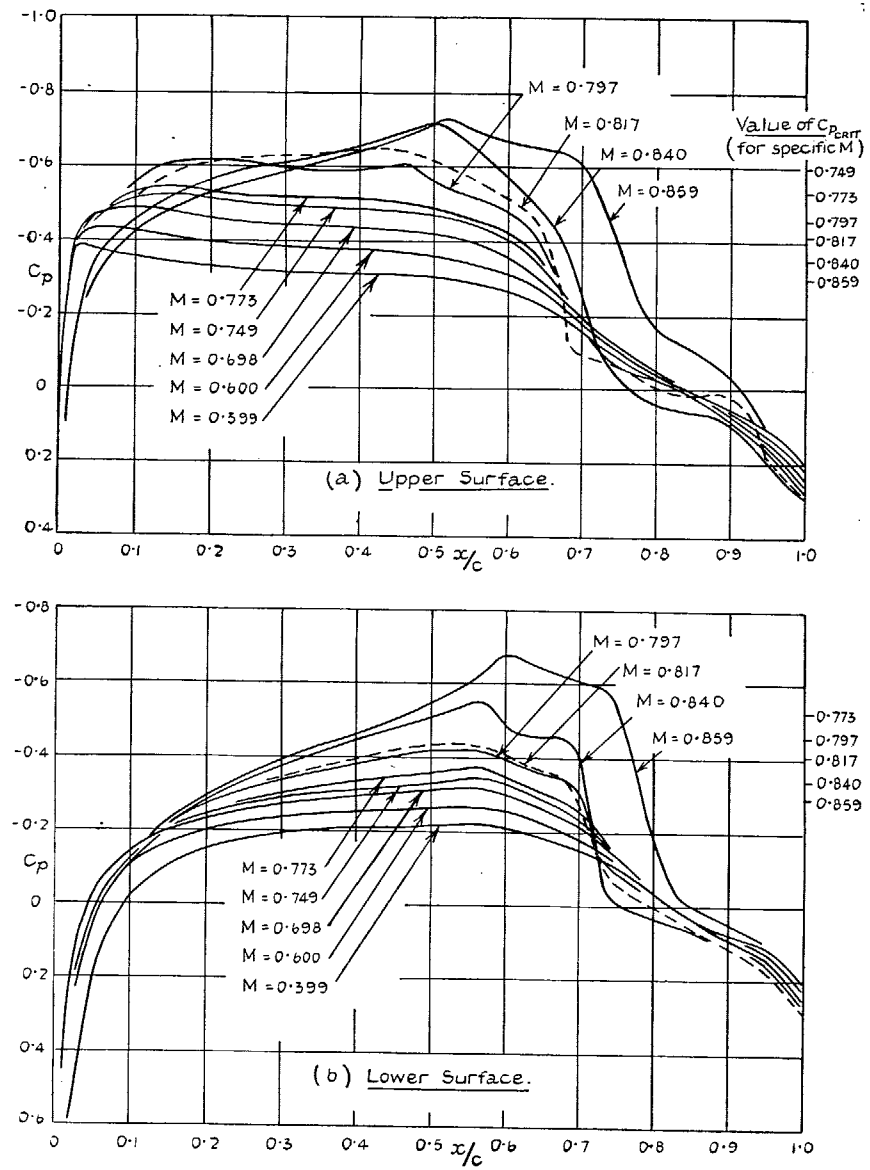

FIG. 4. 10 per cent RAE 104 aerofoil : pressure distributions at $\alpha = 1$ deg.

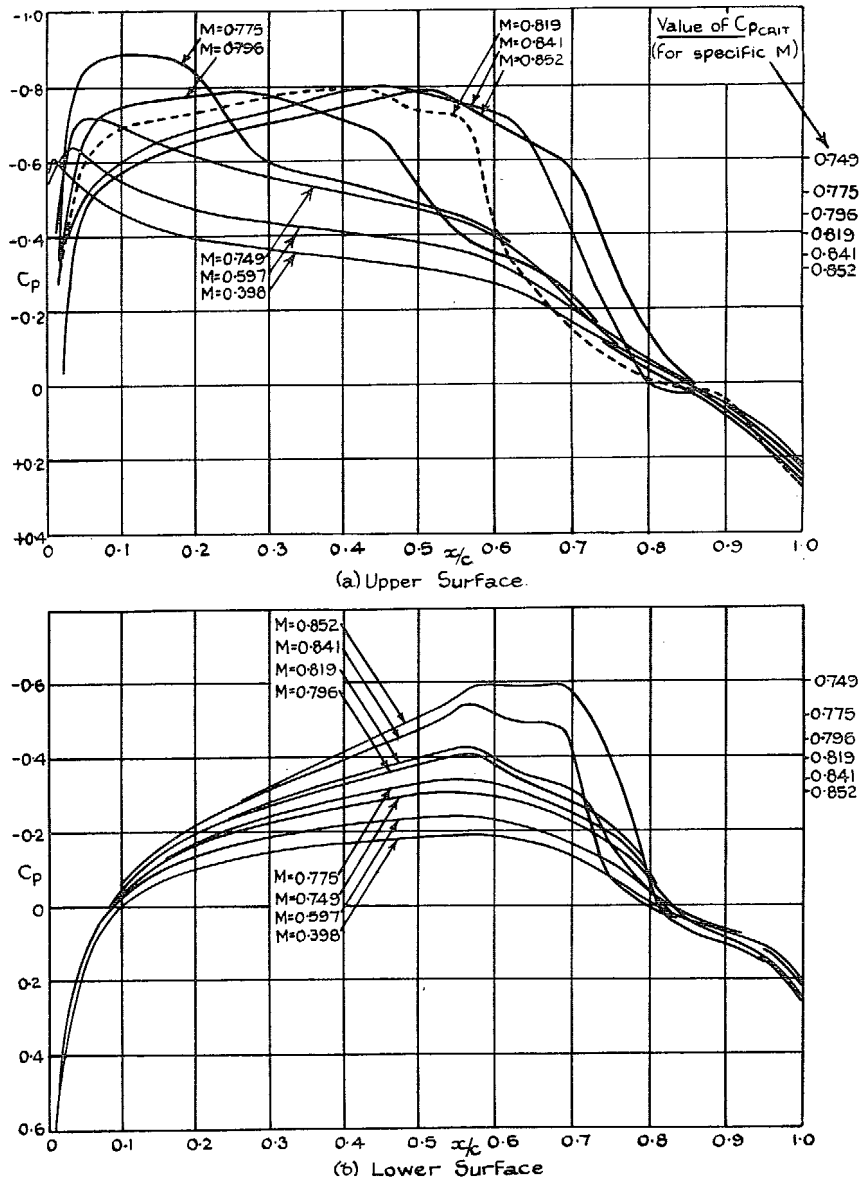

FIG. 5. 10 per cent RAE 104 aerofoil : pressure distributions at $\alpha = 2$ deg.

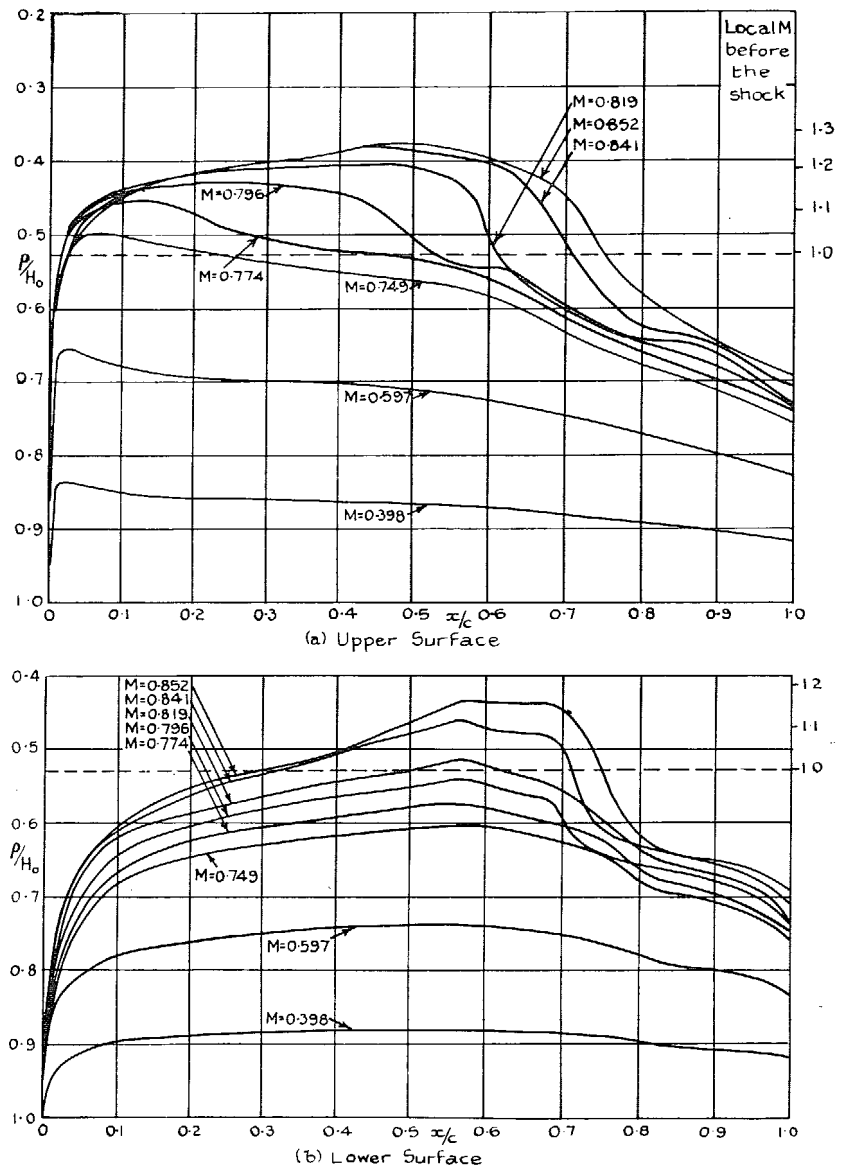

FIG. 6. 10 per cent RAE 104 aerofoil : pressure distributions at $\alpha = 2$ deg.

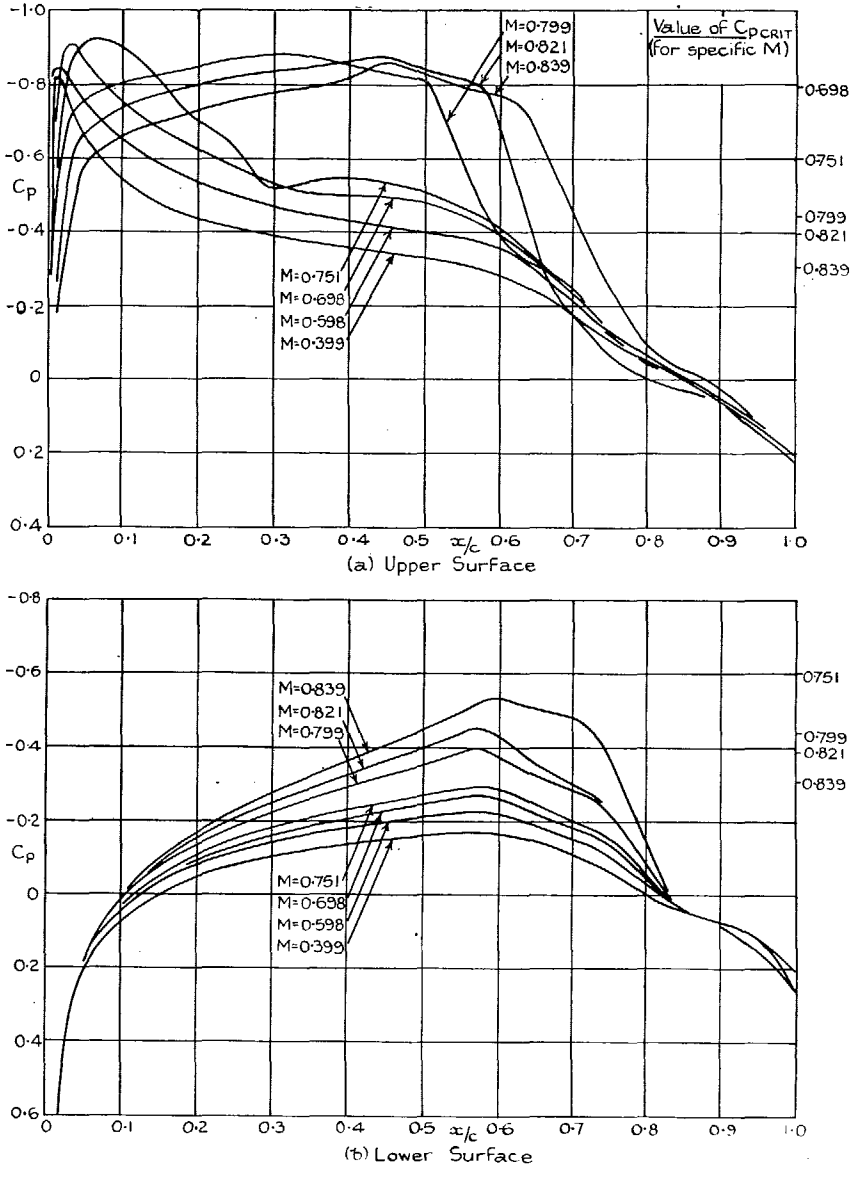

FIG. 7. 10 per cent RAE 104 aerofoil : pressure distributions at $\alpha = 2{\cdot}5$ deg.

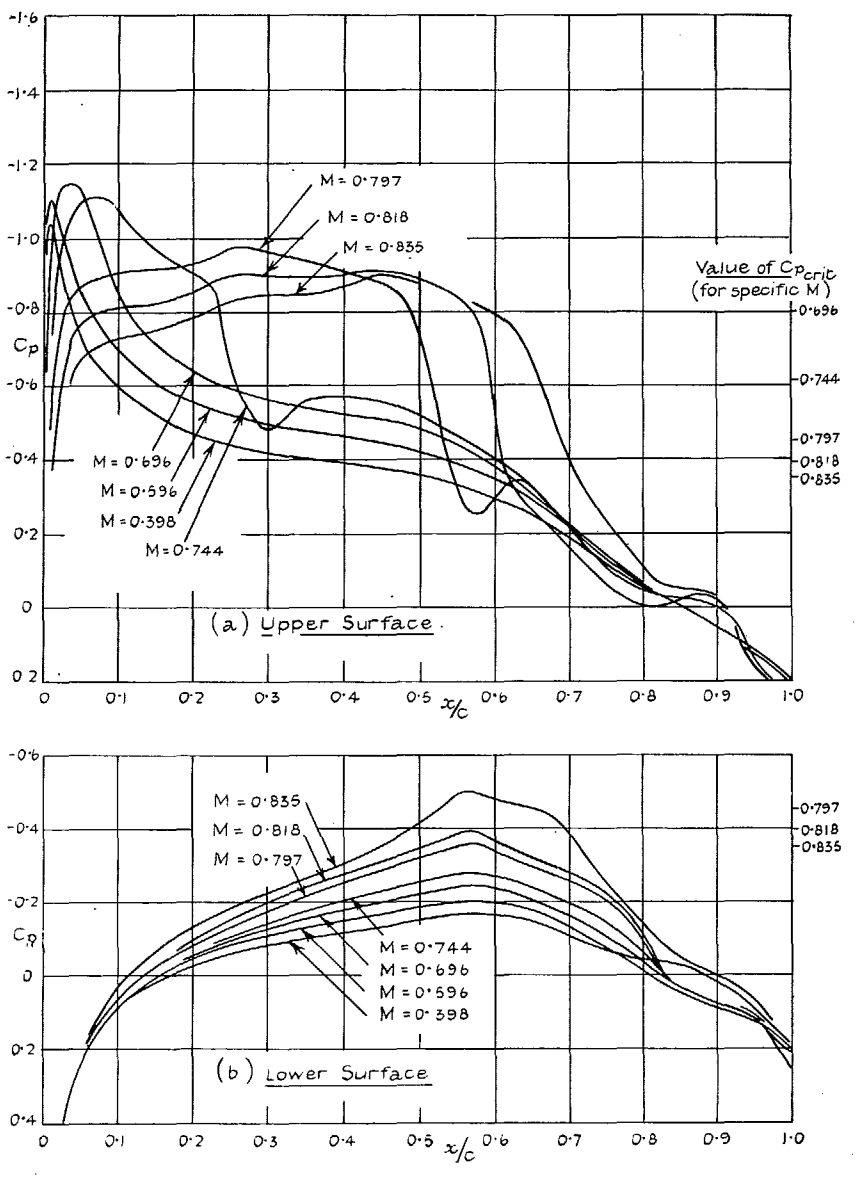

FIG. 8. 10 per cent RAE 104 aerofoil : pressure distributions at $\alpha = 3$ deg.

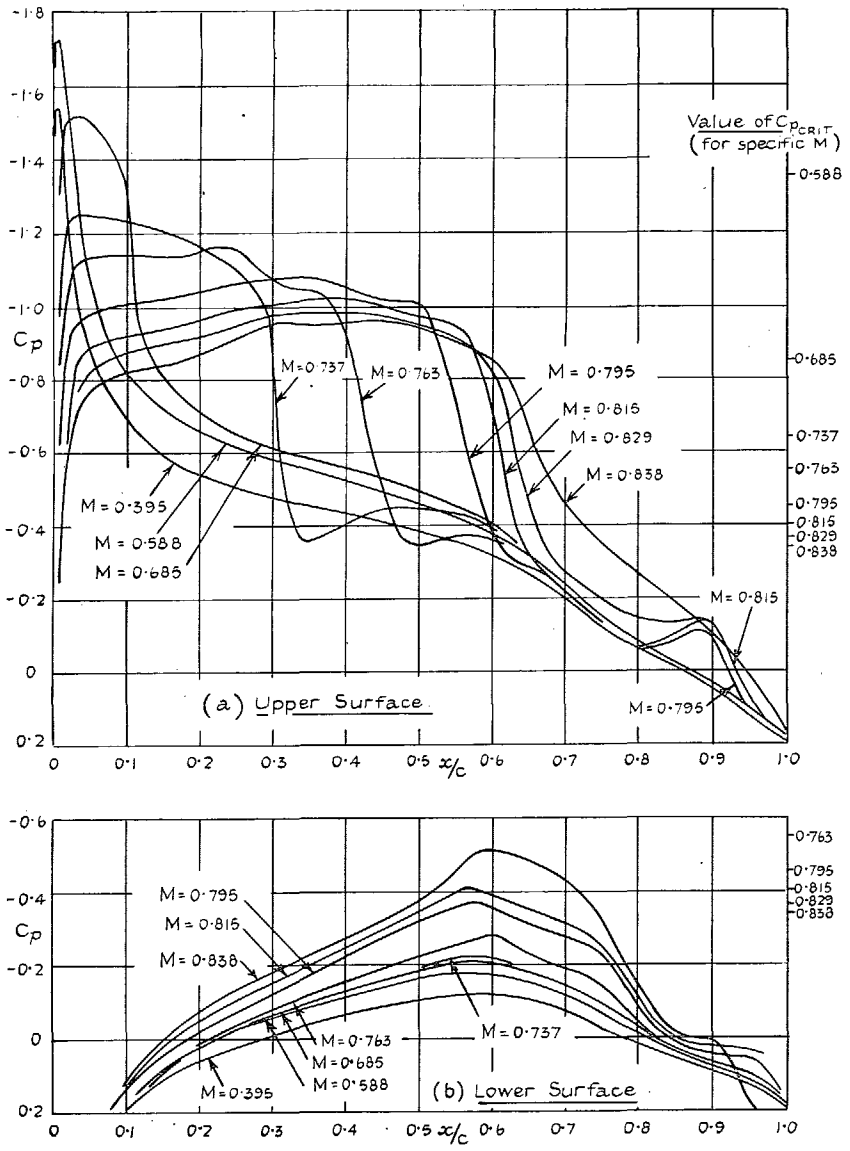

FIG. 9. 10 per cent RAE 104 aerofoil : pressure distributions at $\alpha = 4$ deg.

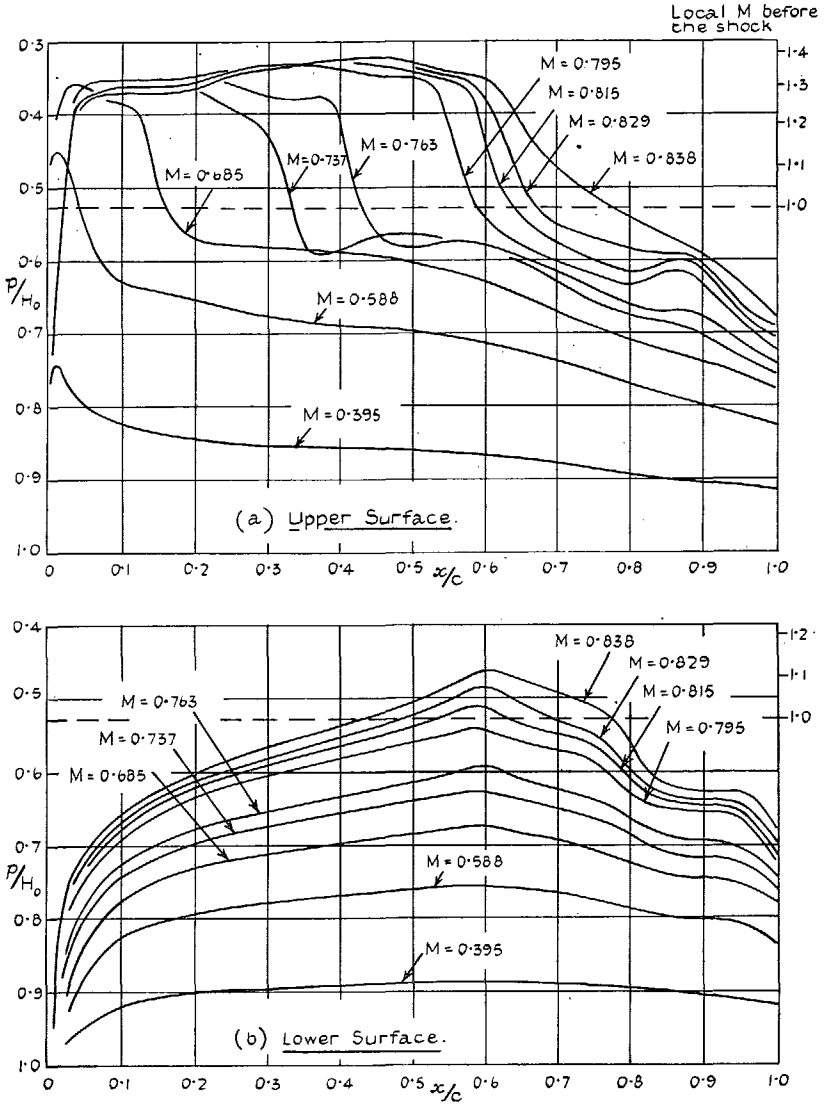

FIG. 10. 10 per cent RAE 104 aerofoil : pressure distributions at $\alpha = 4$ deg.

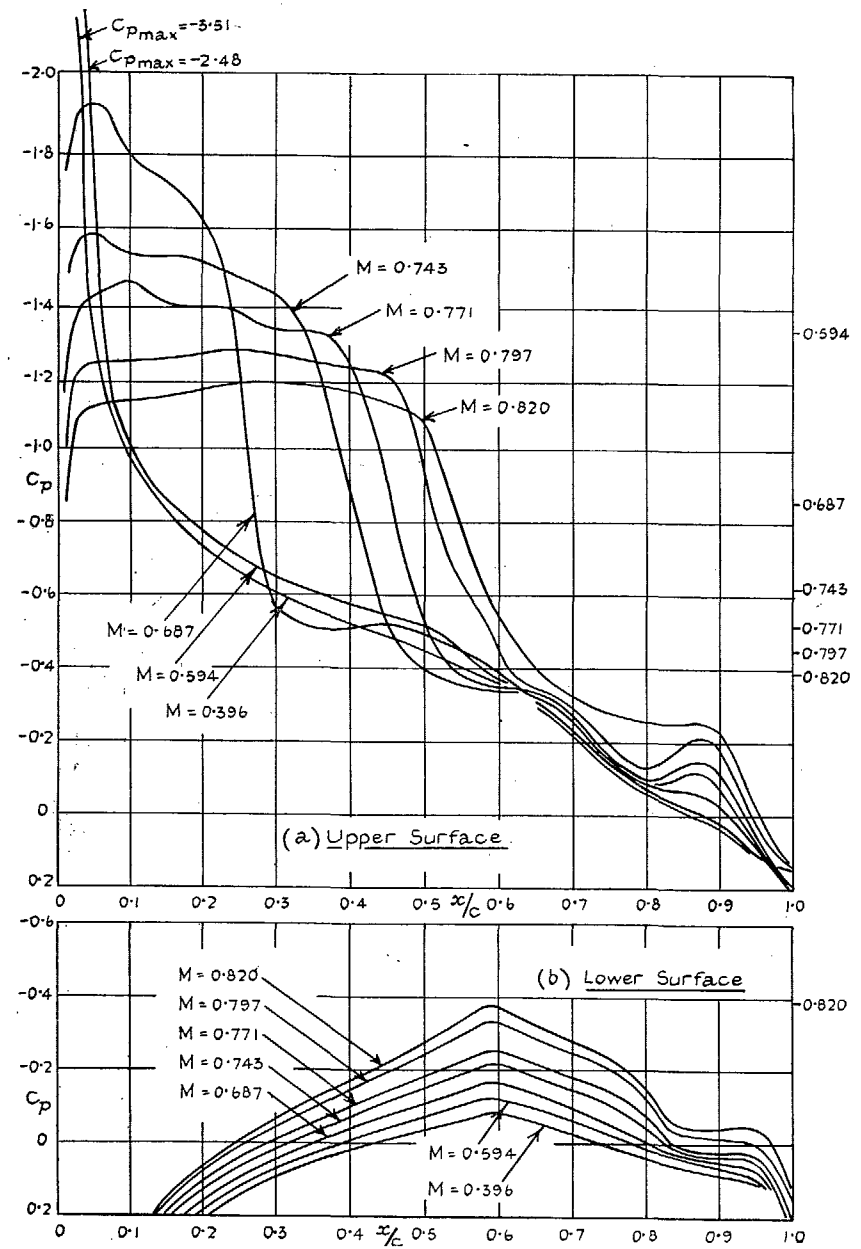

FIG. 11. 10 per cent RAE 104 aerofoil : pressure distributions at $\alpha = 6$ deg.

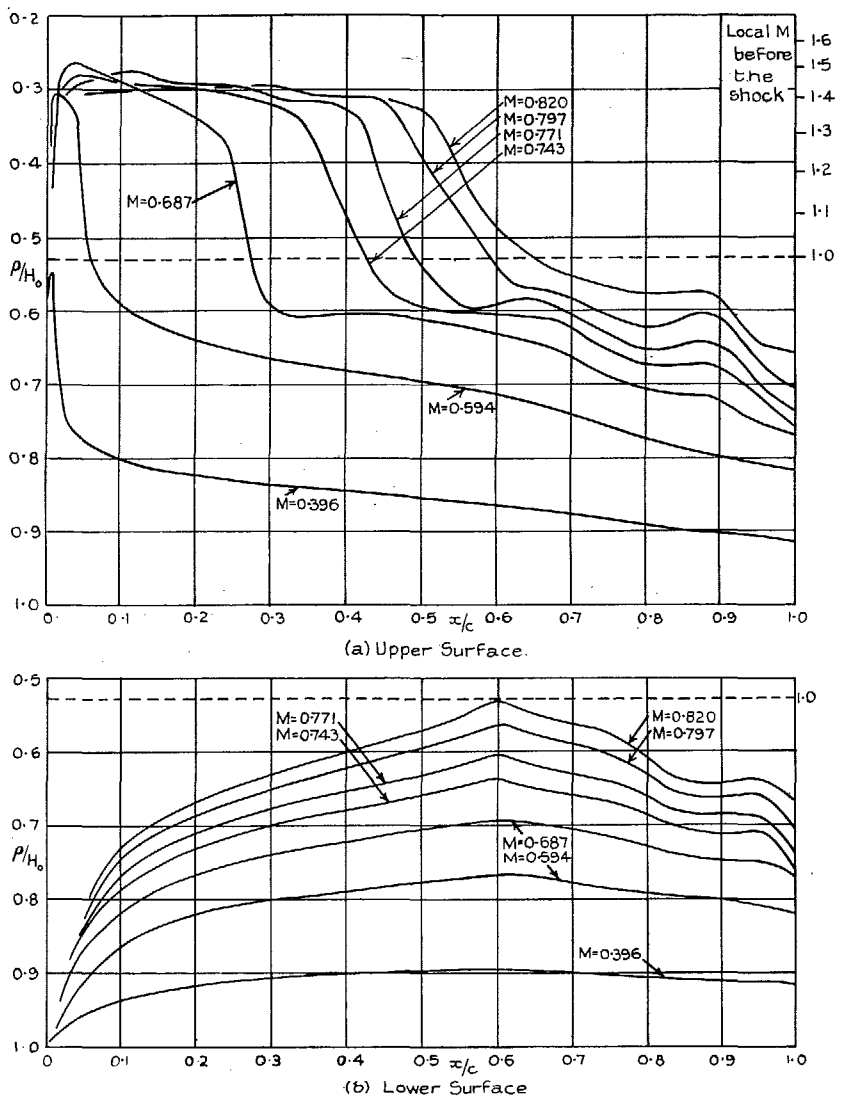

FIG. 12. 10 per cent RAE 104 aerofoil : pressure distributions at $\alpha = 6$ deg.

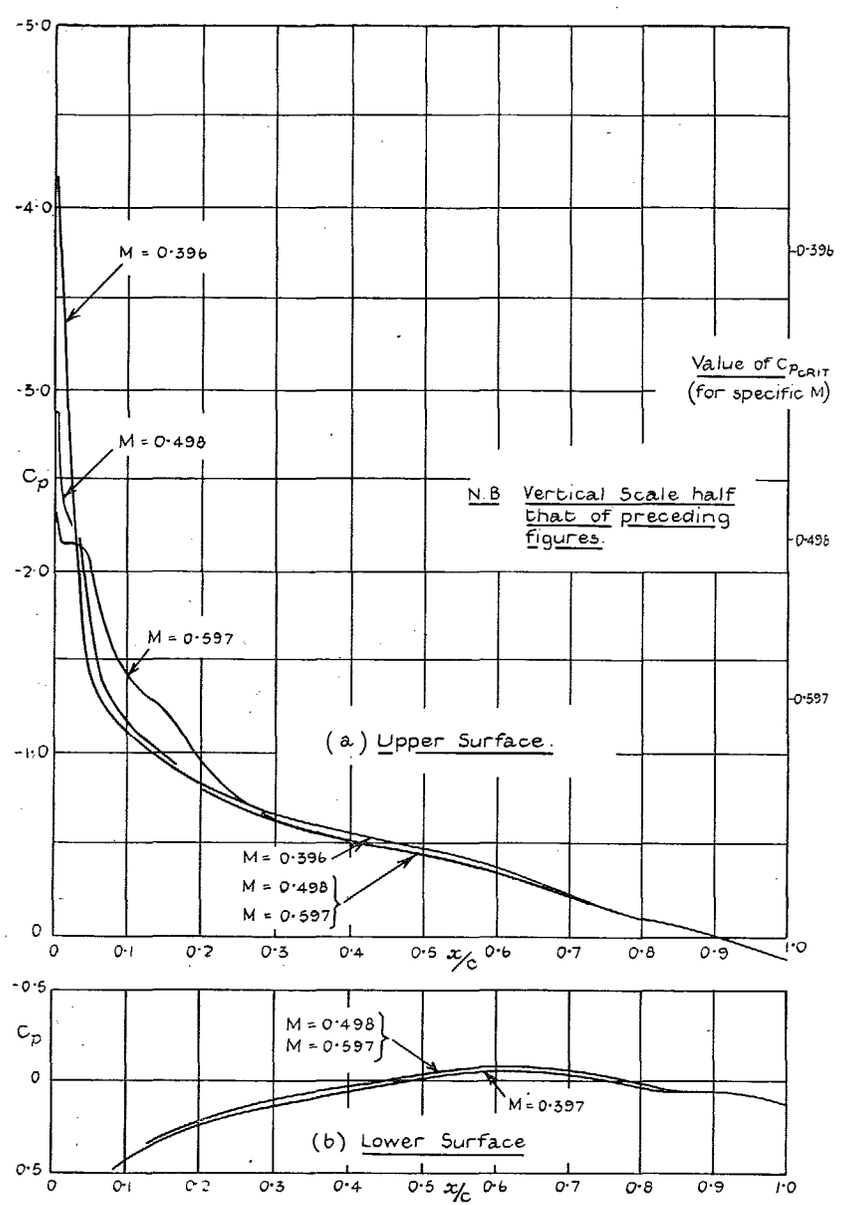

FIG. 13. 10 per cent RAE 104 aerofoil : pressure distributions at $\alpha = 7$ deg.

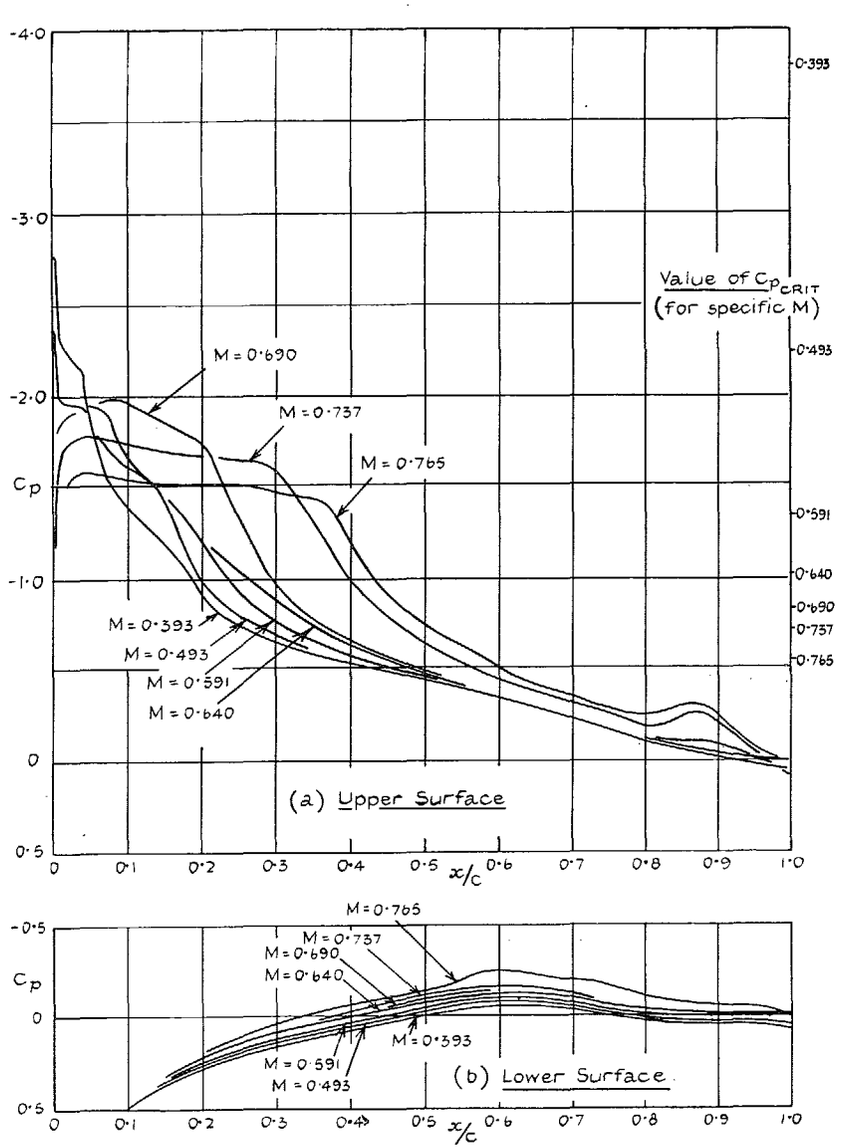

FIG. 14. 10 per cent RAE 104 aerofoil : pressure distributions at $\alpha = 8$ deg.

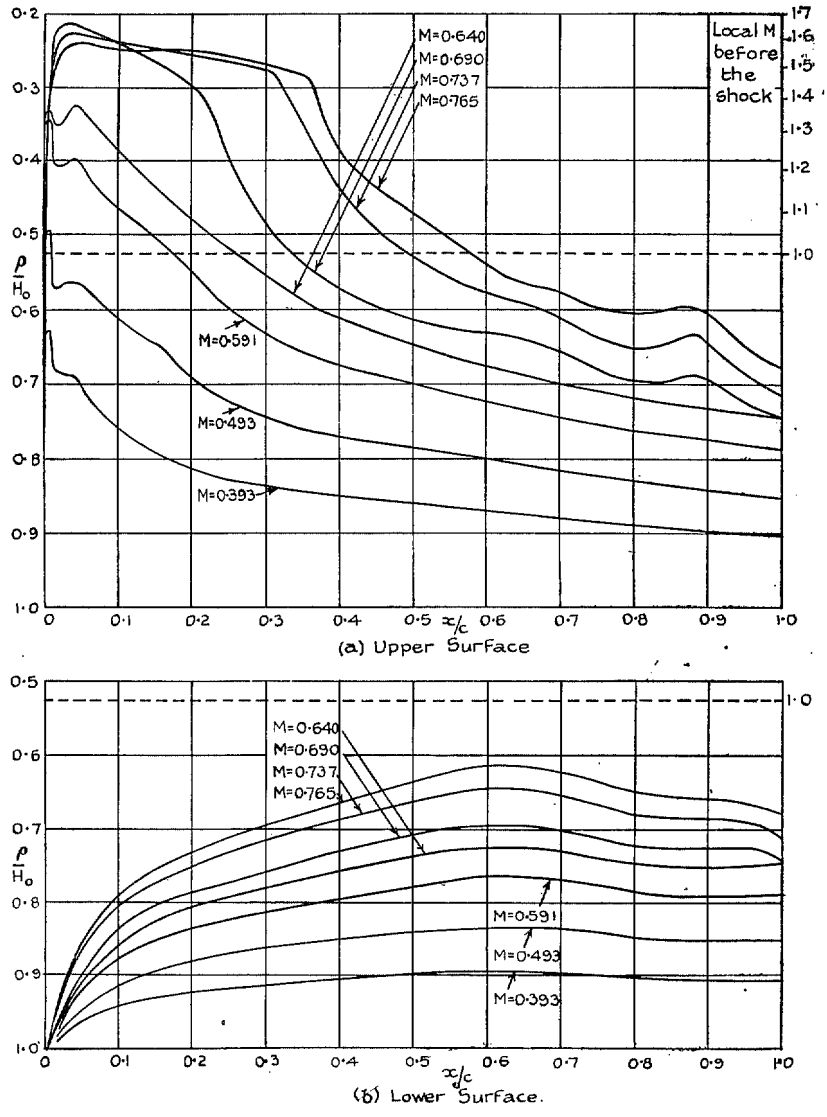

FIG. 15. 10 per cent RAE 104 aerofoil : pressure distributions at $\alpha = 8$ deg.

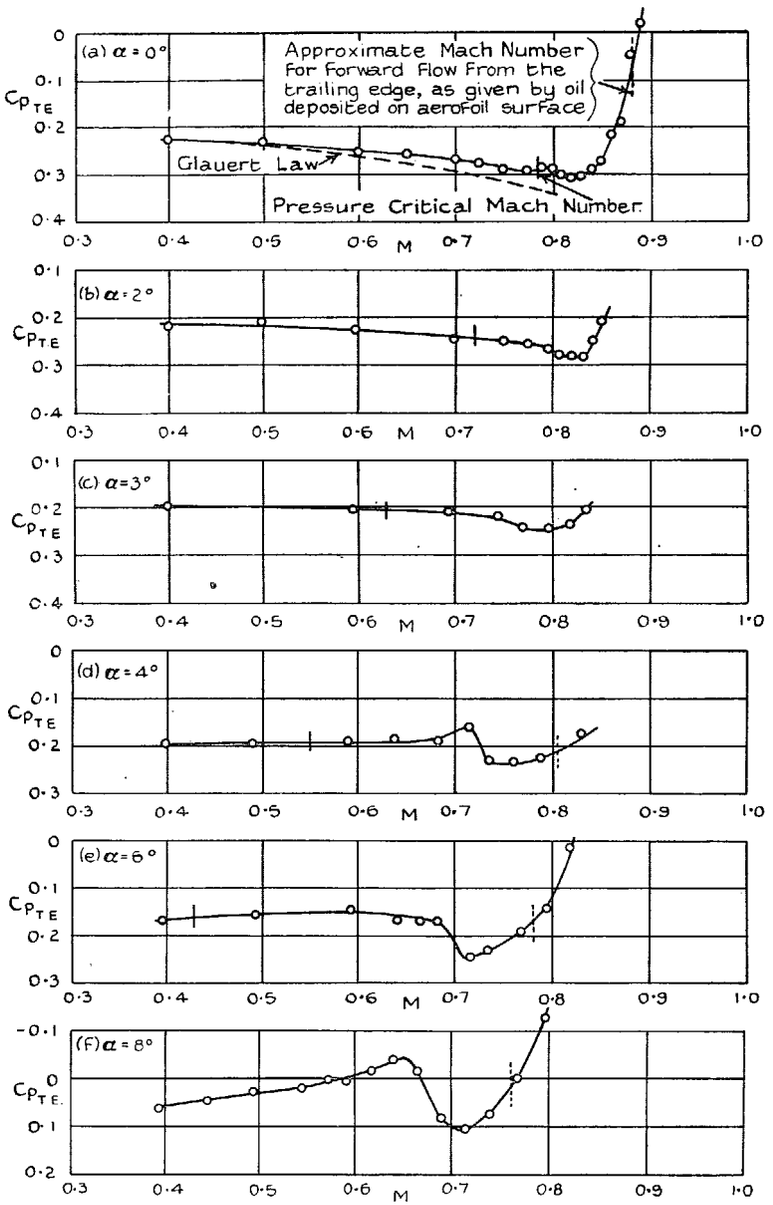

FIG. 16. Variation of pressure coefficient at the trailing edge with Mach number for a range of incidence.

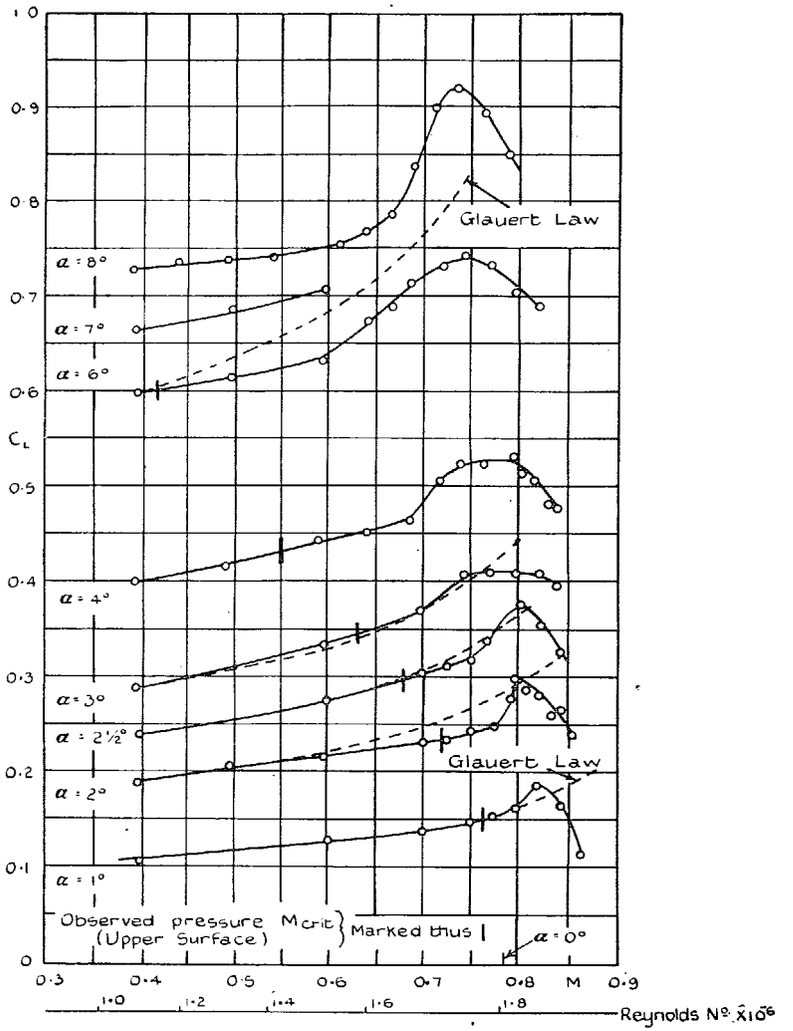

FIG. 17. Variation of C_L with Mach number at constant incidence.

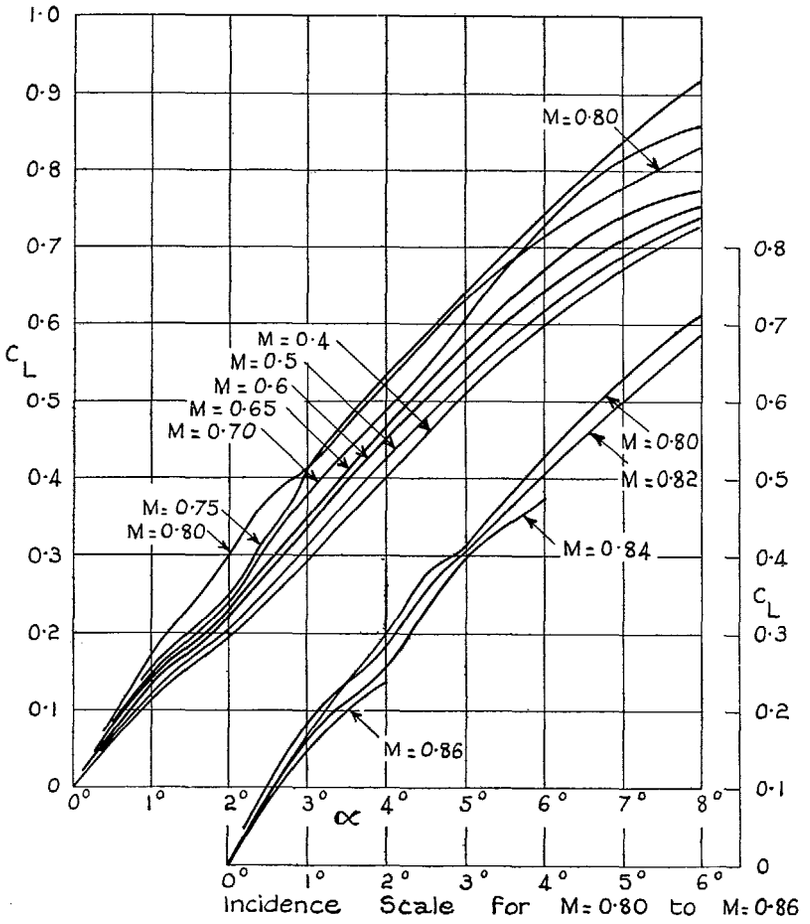

FIG. 18. Variation of C_L with incidence at constant Mach number.

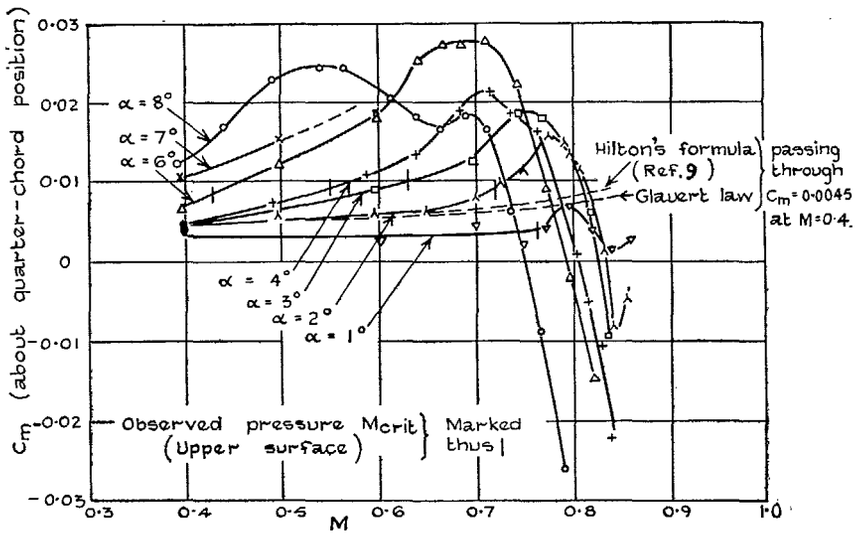

FIG. 19. Variation of C_m with Mach number at constant incidence.

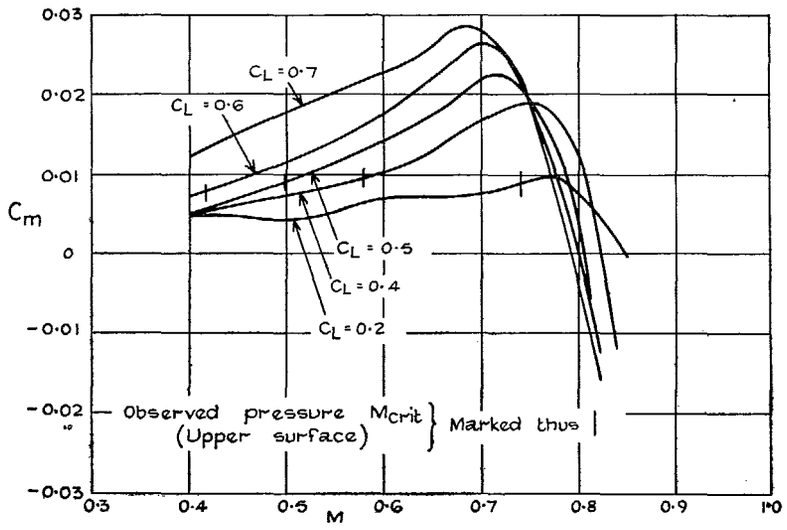

FIG. 20. Variation of C_m with Mach number constant at C_L.

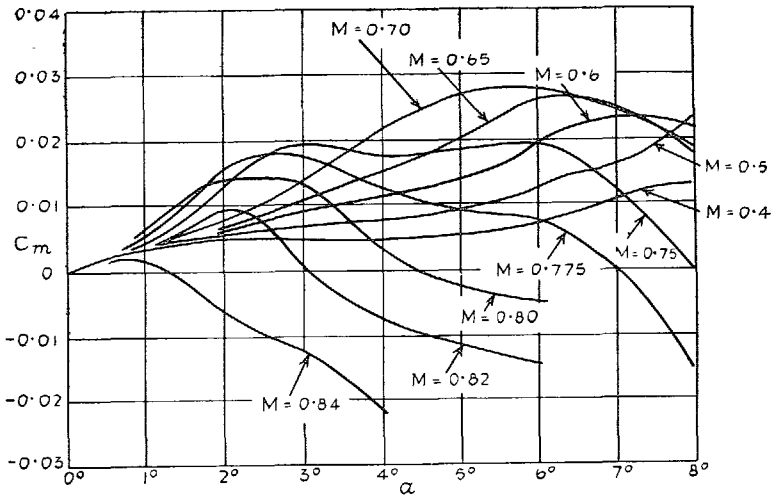

FIG. 21. Variation of C_m with incidence at constant Mach number.

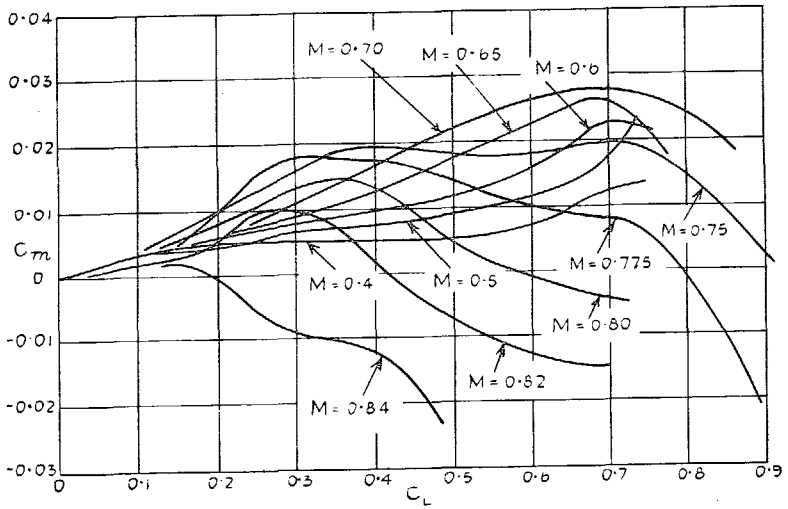

FIG. 22. Variation of C_m with C_L at constant Mach number.

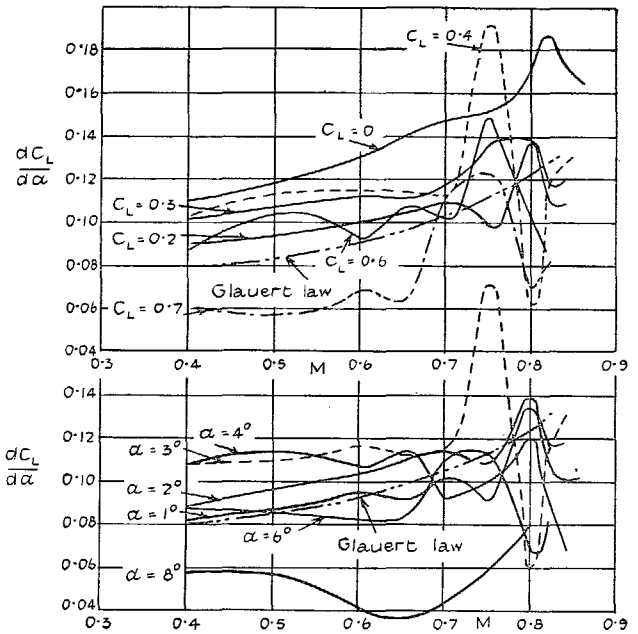

FIG. 23. Variation of $dC_L/d\alpha$ with M at constant C_L or α.

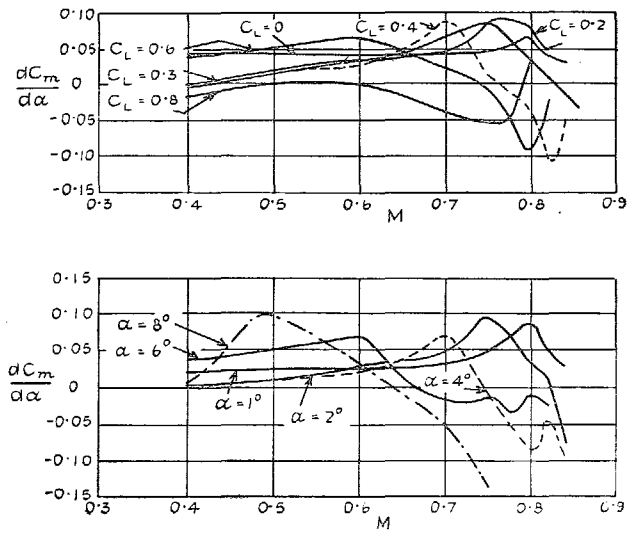

FIG. 24. Variation of $dC_m/d\alpha$ with M at constant C_L or α.

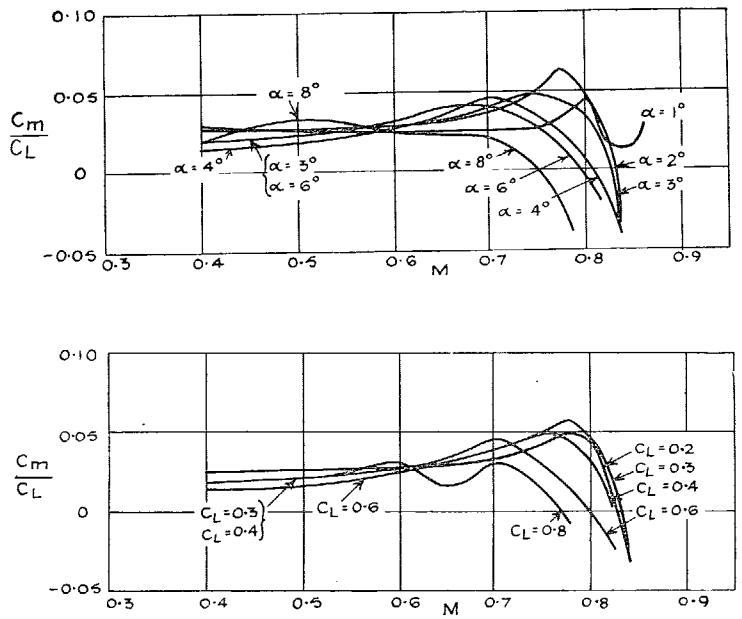

FIG. 25. Variation of C_m/C_L (centre of pressure distance forward of quarter-chord) with M at constant incidence and lift coefficient.

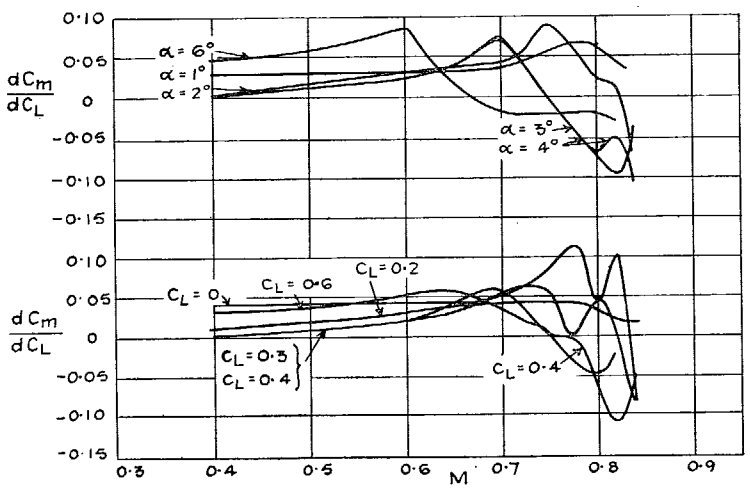

FIG. 26. Variation of dC_m/dC_L (aerodynamic-centre position forward of quarter-chord) with M at constant incidence and lift coefficient.

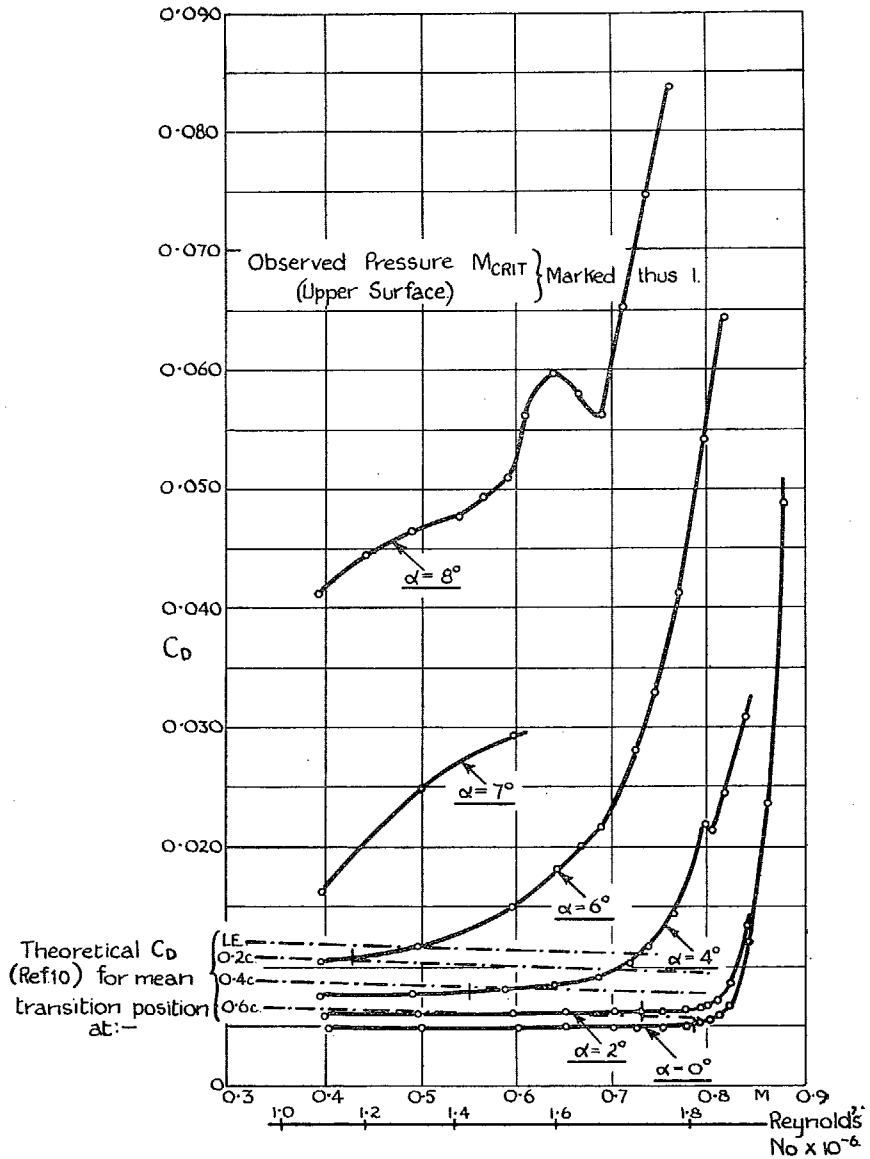

FIG. 27. Variation of C_D with Mach number at constant incidence.

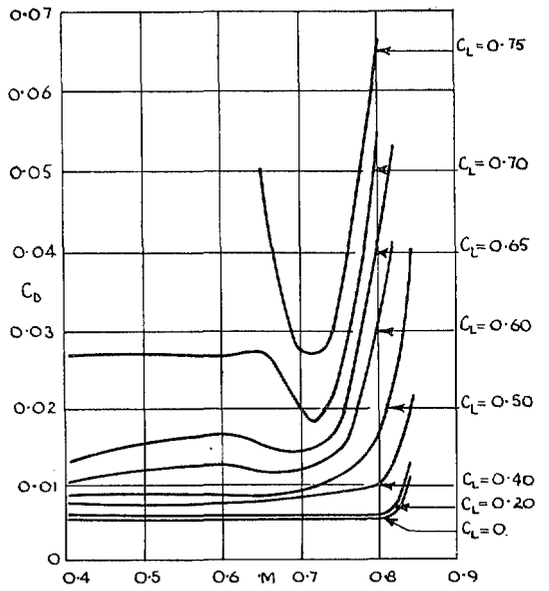

FIG. 28. Variation of C_D with M at constant C_L.

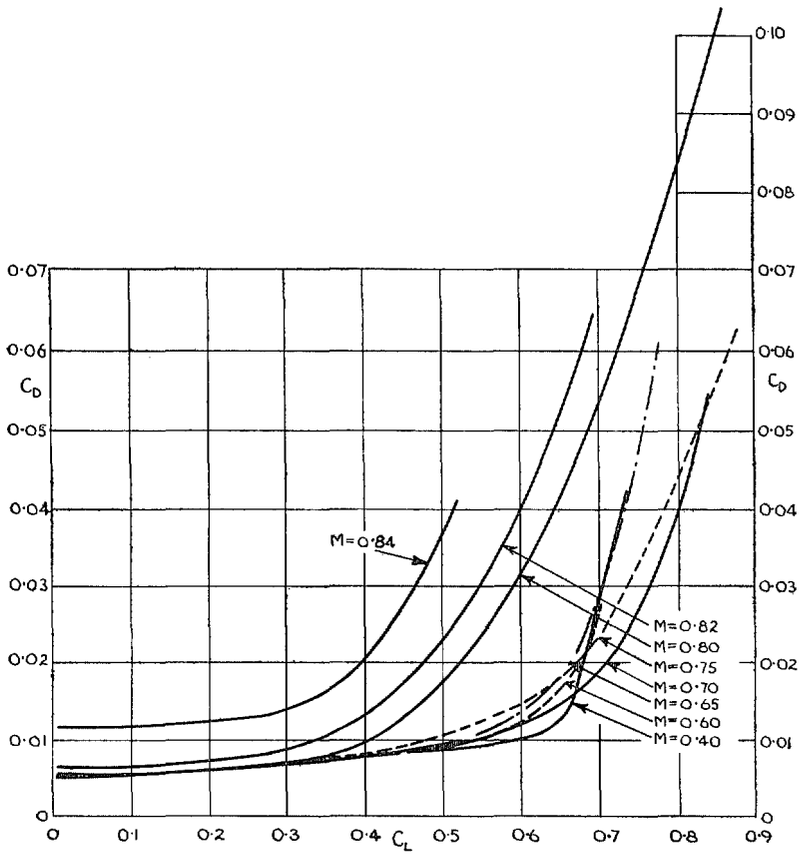

FIG. 29. Variation of C_D with C_L at constant Mach number.

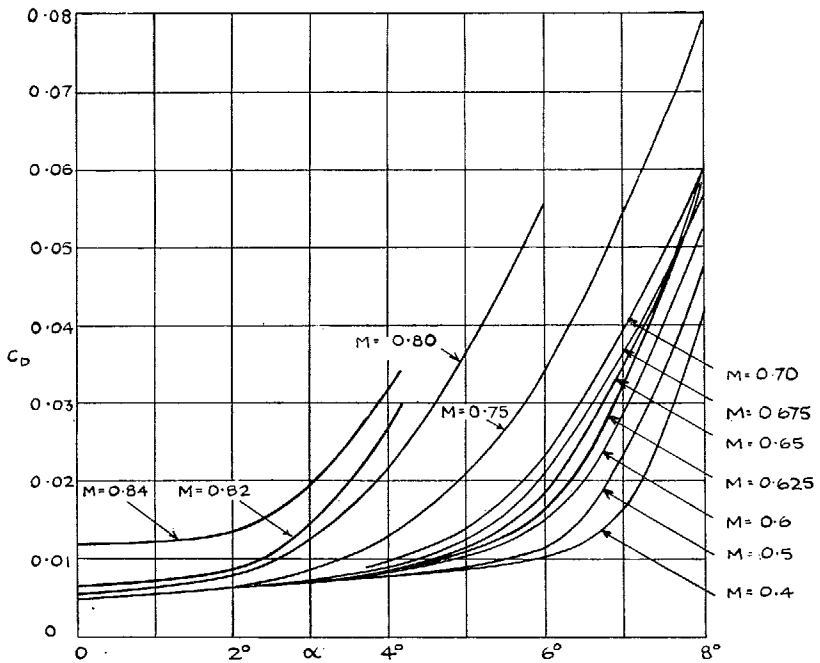

FIG. 30. Variation of C_D with incidence at constant Mach number.

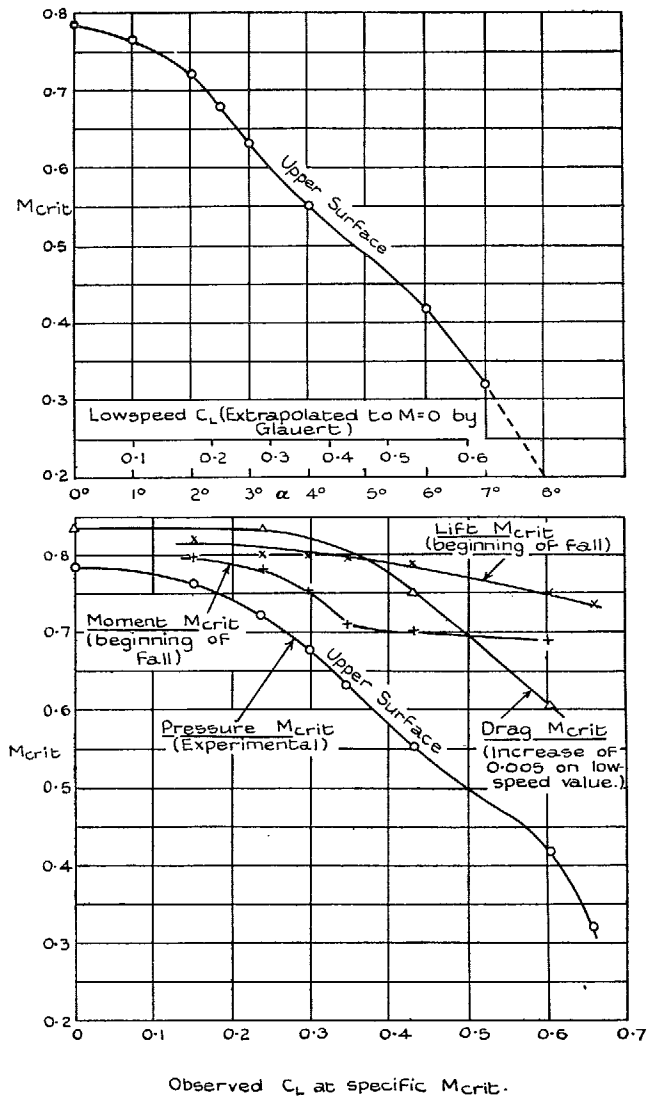

FIG. 31. Variation of critical Mach number with lift coefficient and incidence.

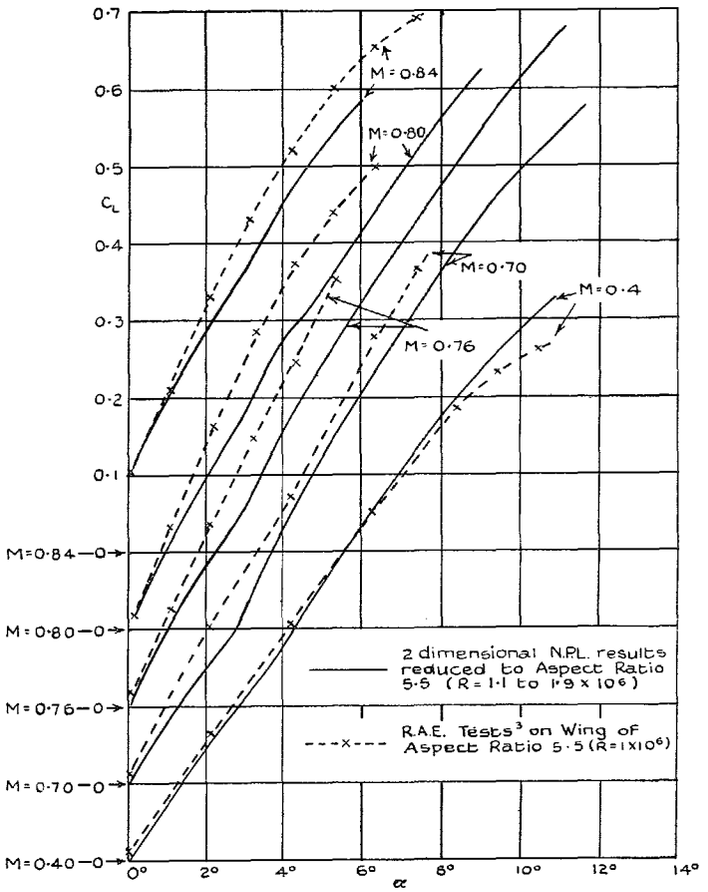

FIG. 32. Comparison of N.P.L. and R.A.E. tests on RAE 104 at aspect ratio 5·5.

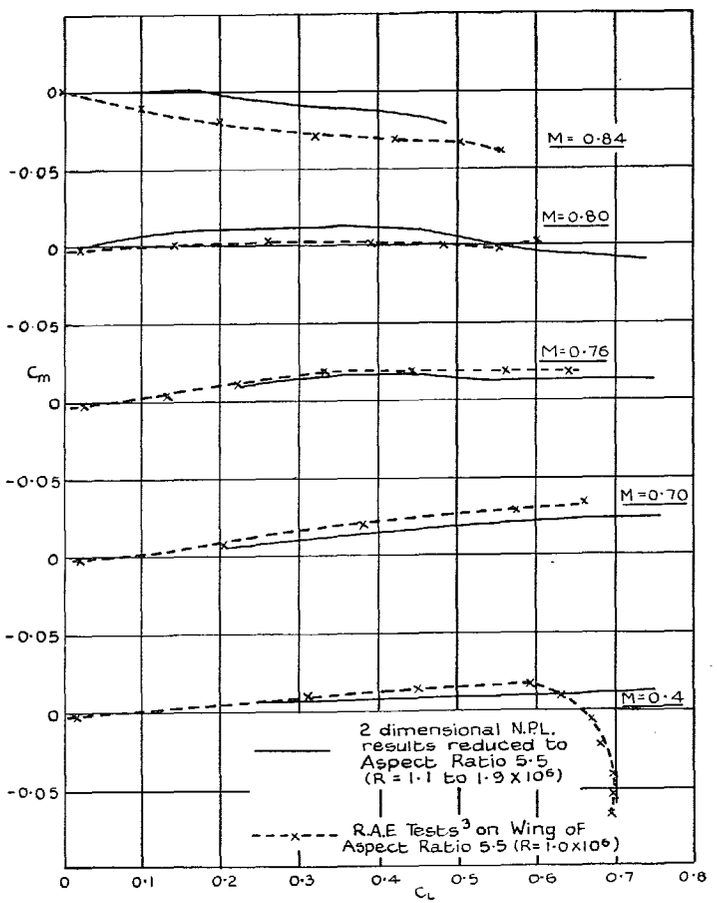

FIG. 33. Comparison of N.P.L. and R.A.E. results on RAE 104 aerofoil.

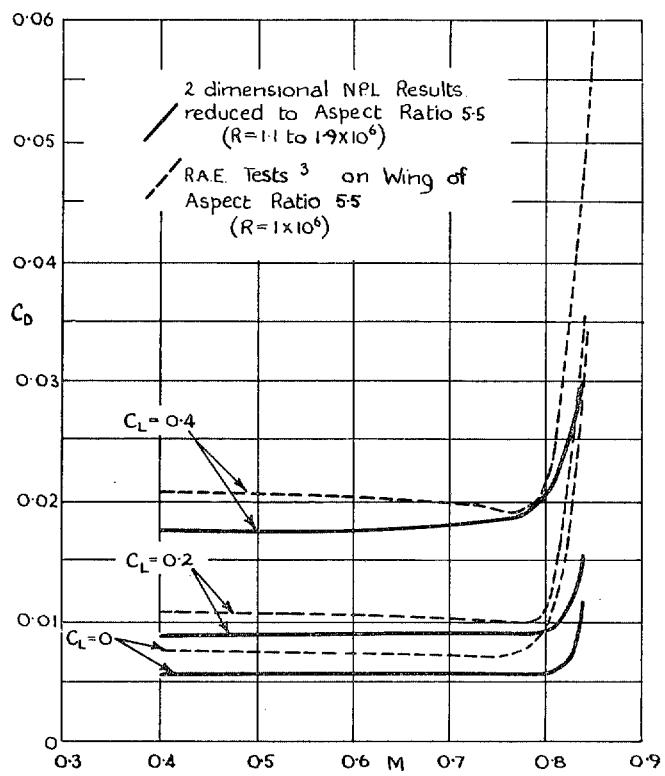

FIG. 34. Comparison of N.P.L. and R.A.E. tests on RAE 104 at aspect ratio 5·5.

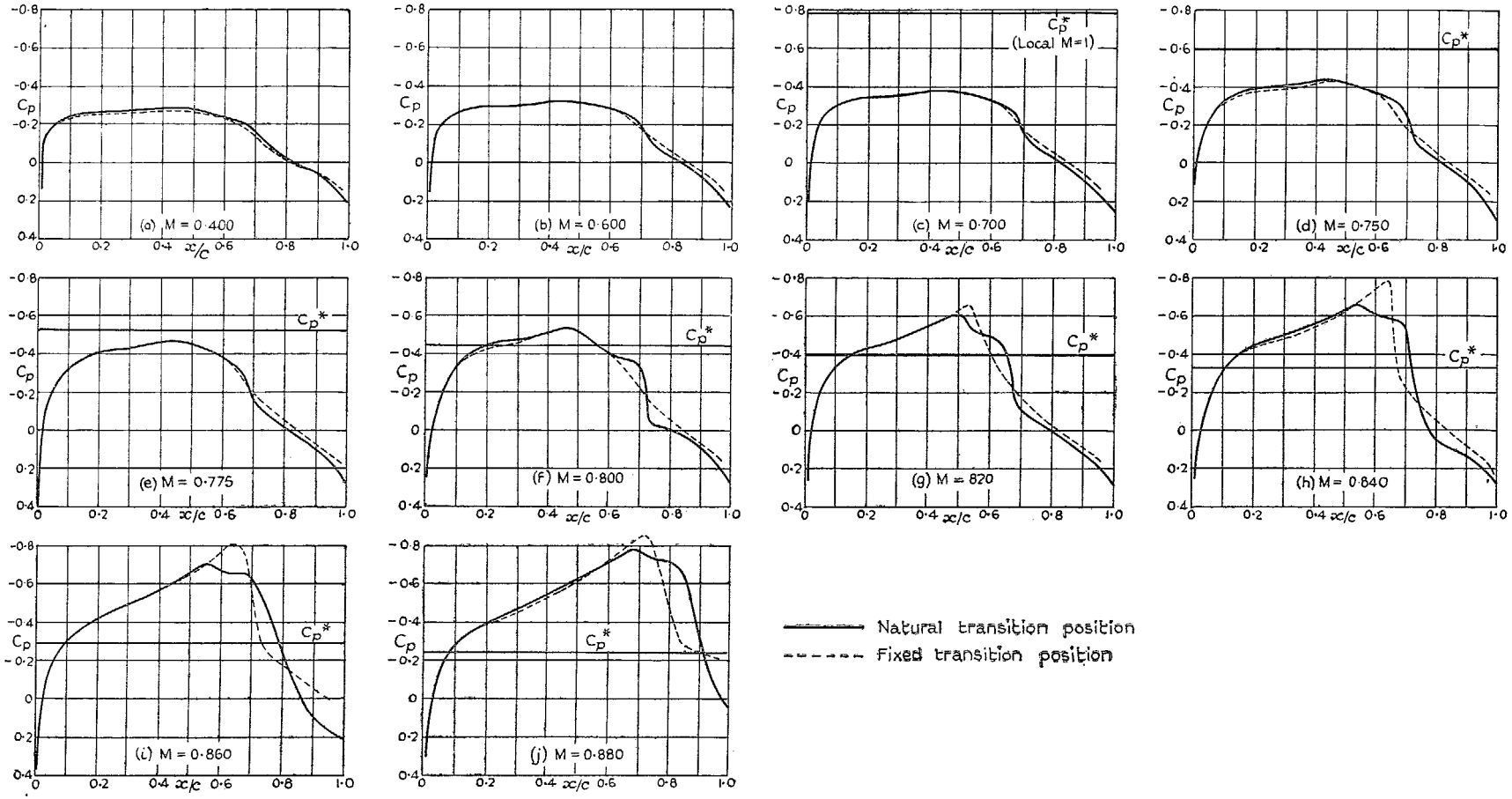

FIG. 35. Comparison of pressure distributions obtained on the aerofoil with and without artificial transition : $\alpha = 0$ deg.

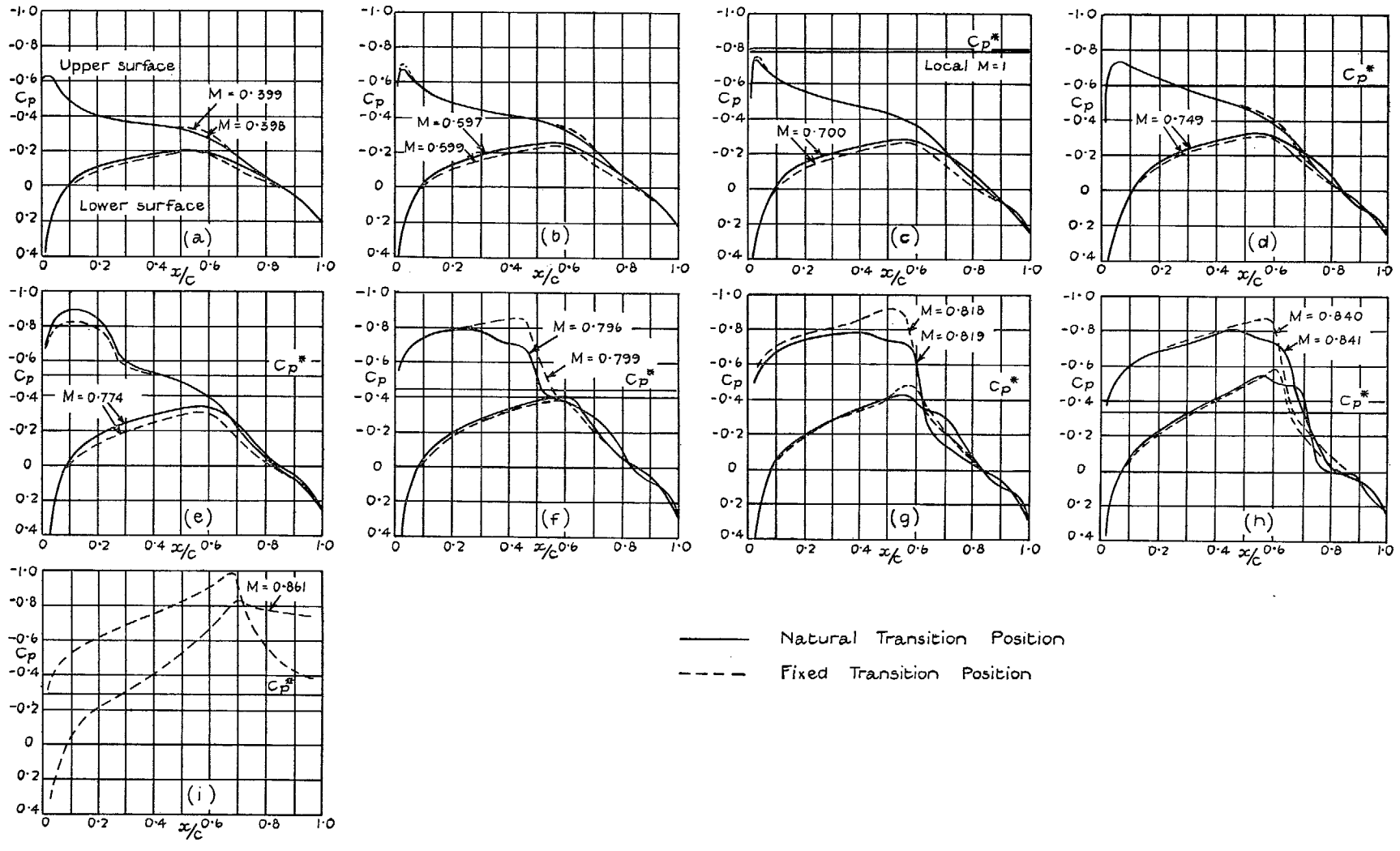

FIG. 36. Comparison of pressure distributions obtained on the aerofoil with and without artificial transition : $\alpha = 2$ deg.

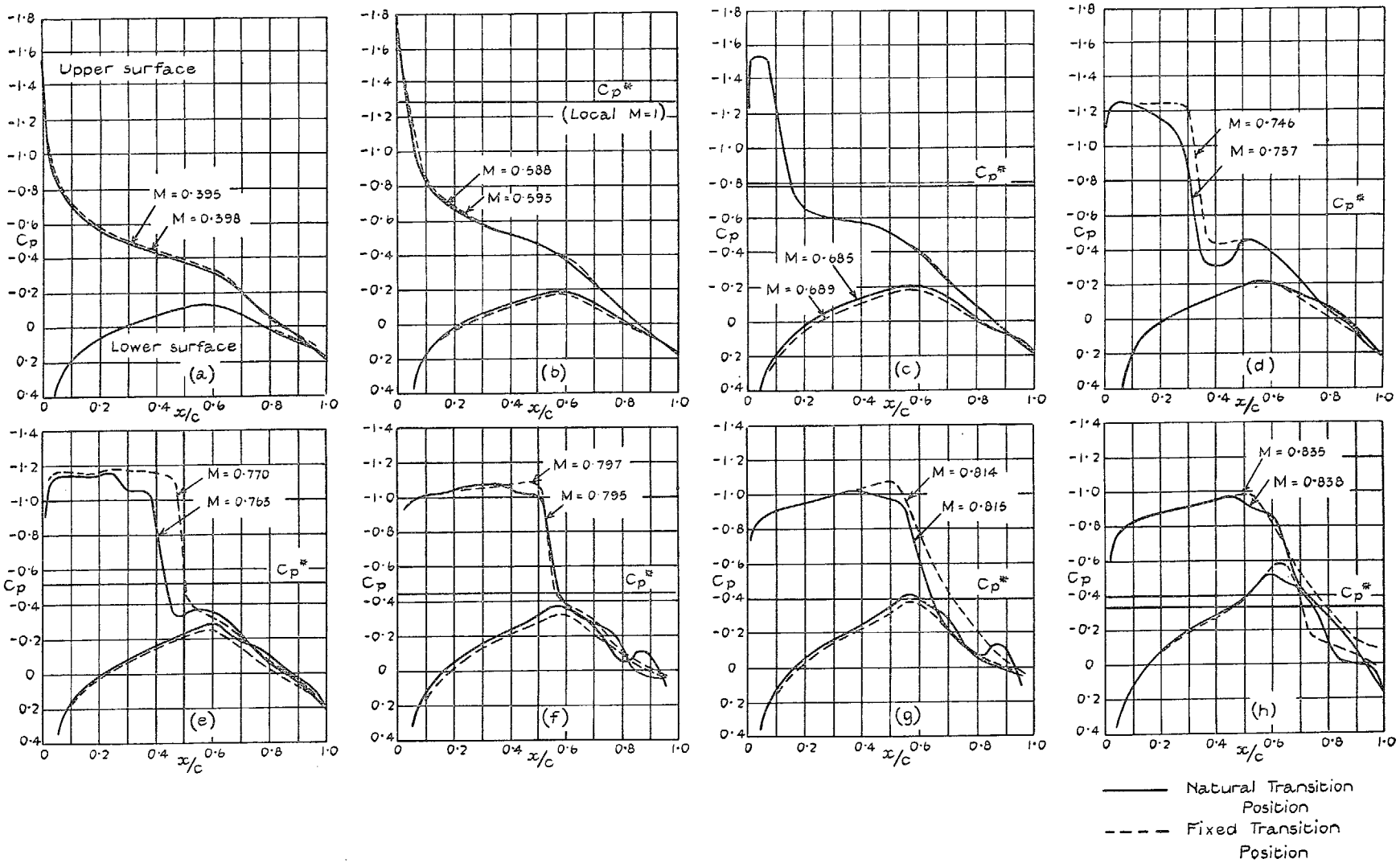

FIG. 37. Comparison of pressure distributions obtained on the aerofoil with and without artificial transition : $\alpha = 4$ deg.

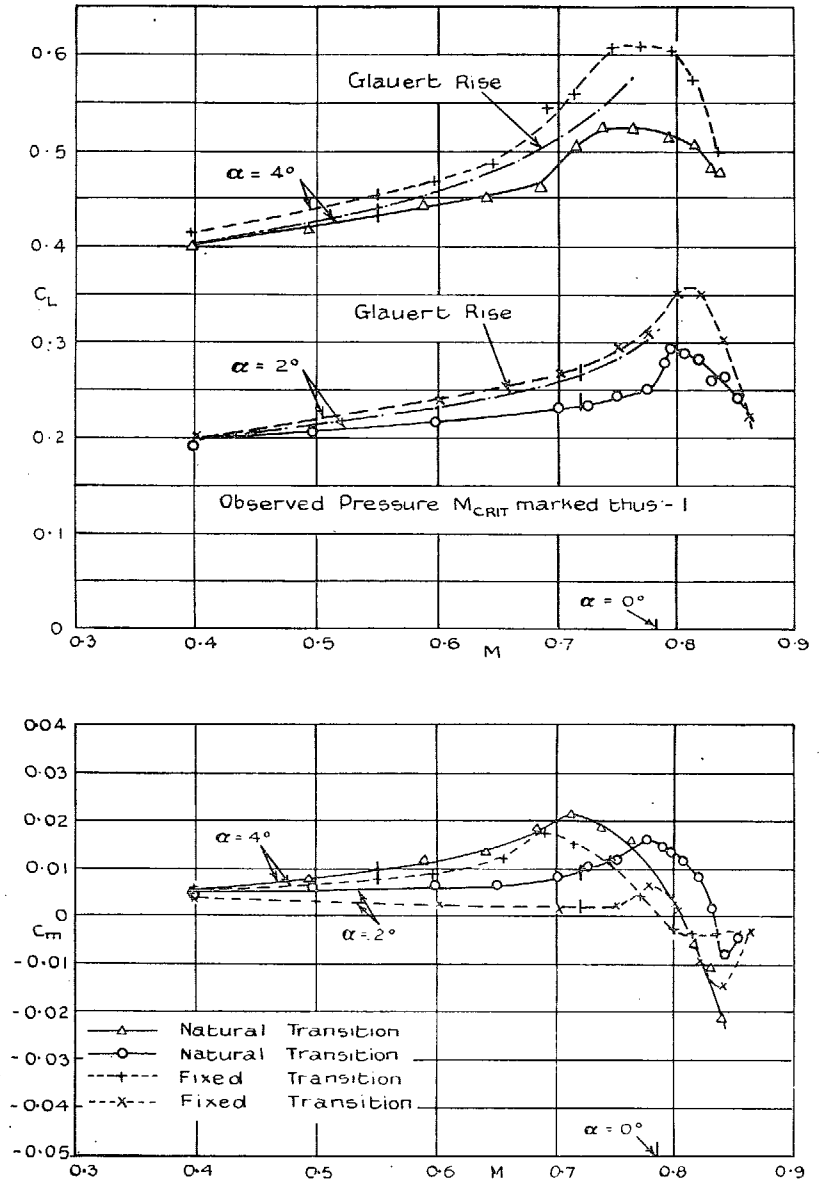

FIG. 38. Variation of C_L and C_m with M for the two sets of tests.

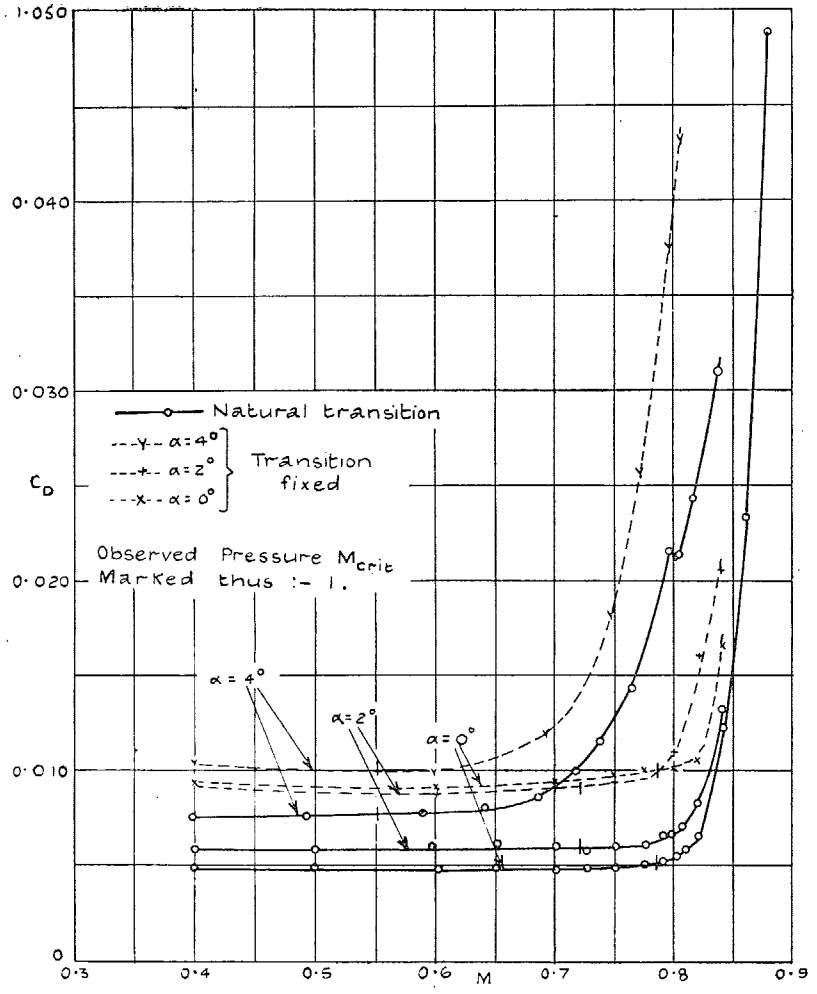

FIG. 39. Variation of C_D with M for the two sets of tests.

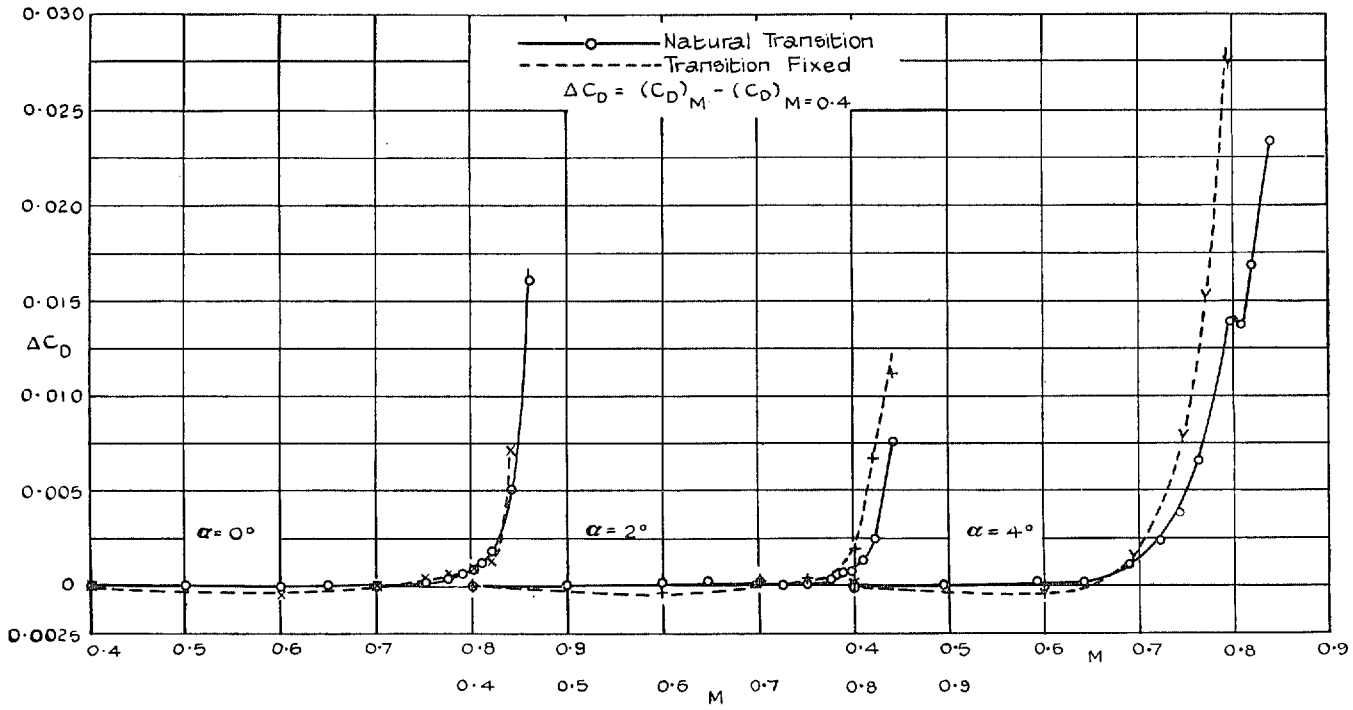

FIG. 40. Variation of ΔC_D with Mach number for the two tests.

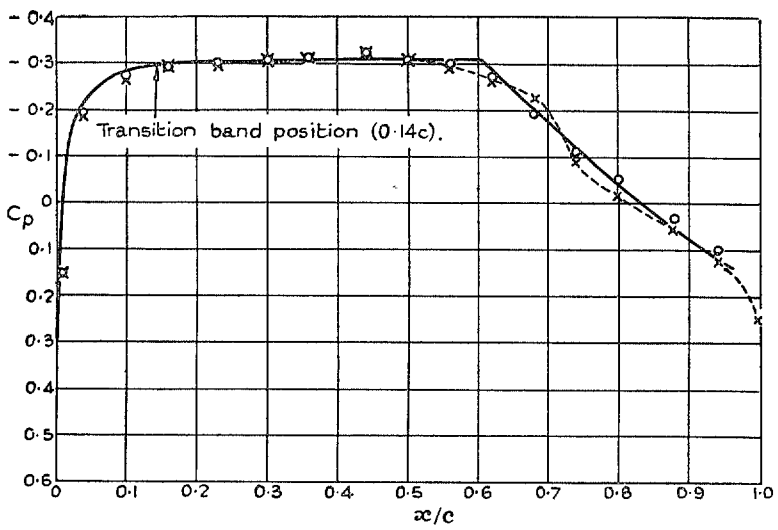

M = 0·600, α = 0°.

o Transition Fixed } Experimental

-----x---- Transition Free }

——— Theoretical (Ref. 4) augmented from incompressible values by Karman-Tsien law.

FIG. 41. Comparison of two experimental pressure distributions with theoretical.

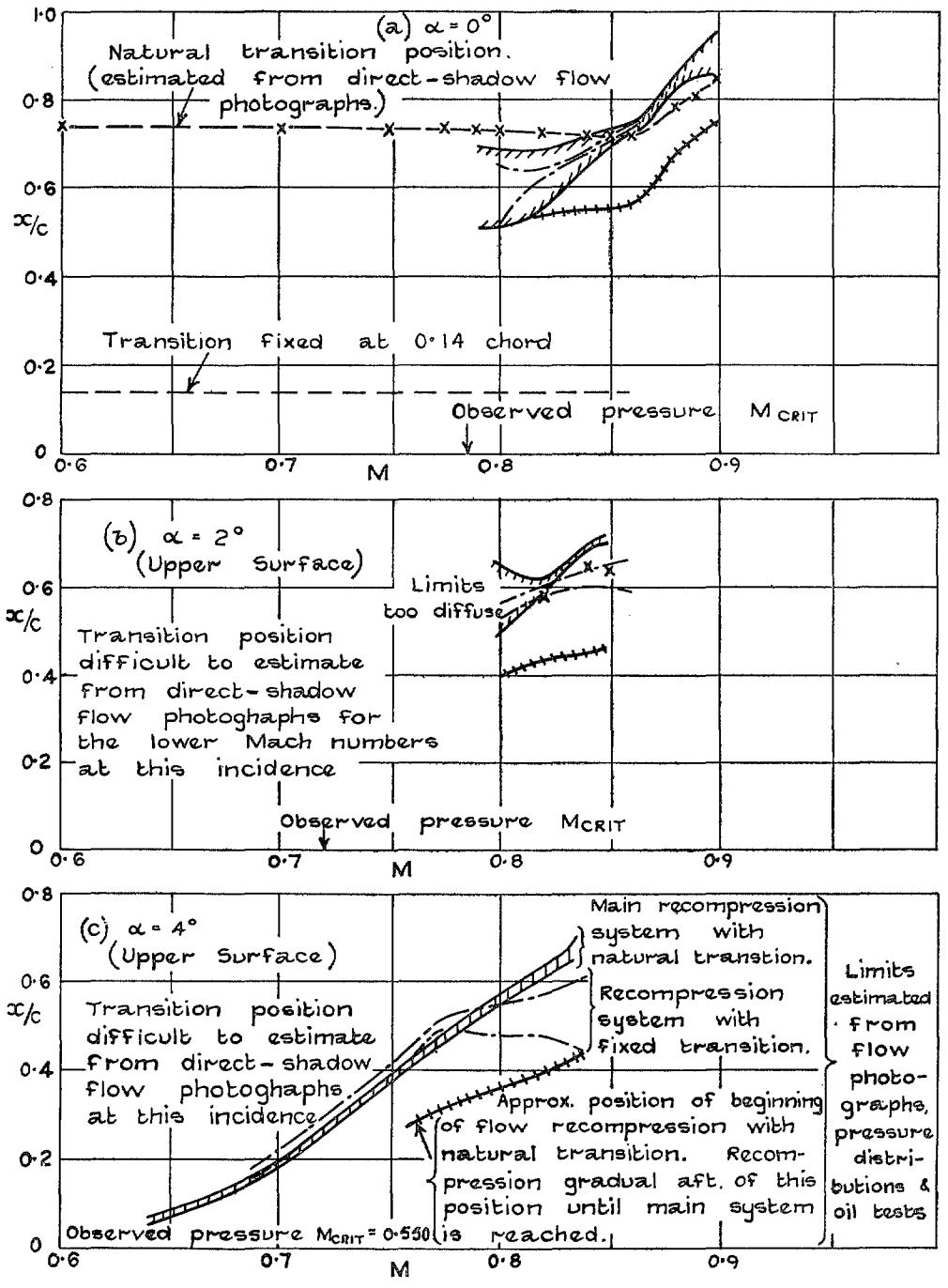

FIG. 42. Variation with Mach number of approximate extent of recompression systems along the aerofoil surface for the two tests.

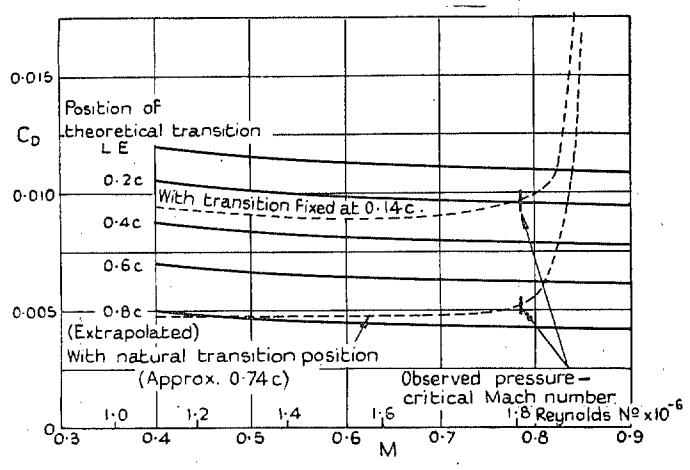

FIG. 43. Comparison of measured values of C_D with theoretical values of Ref. 10 ($\alpha = 0$ deg.)

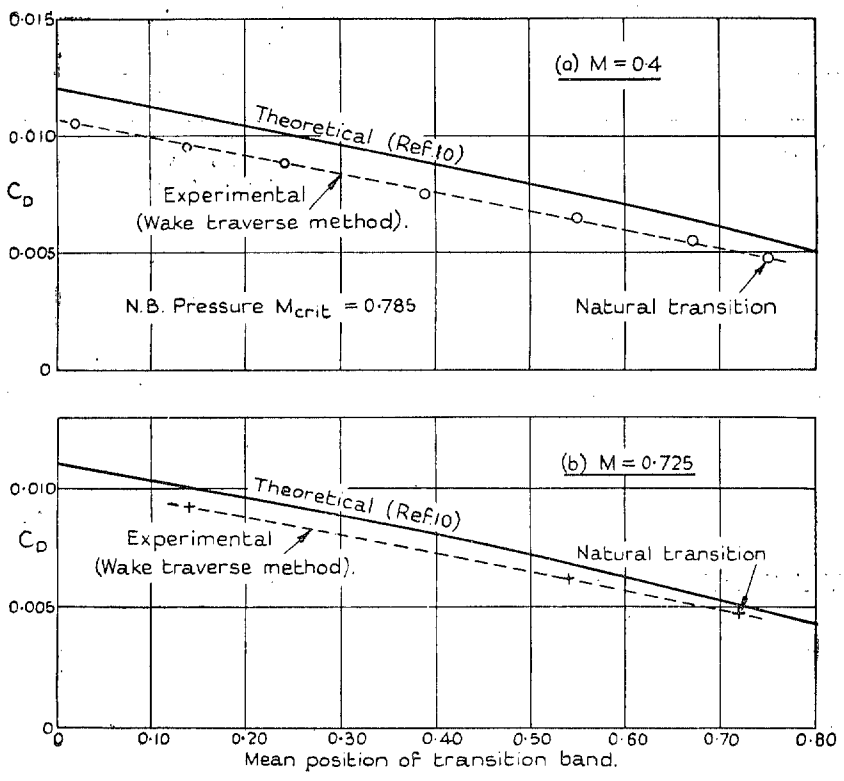

FIG. 44. Variation of profile C_D with position of transition. ($\alpha = 0$ deg.)

Natural transition position

Fixed transition position
(Frigilene band at 0·14 chord on both surfaces)

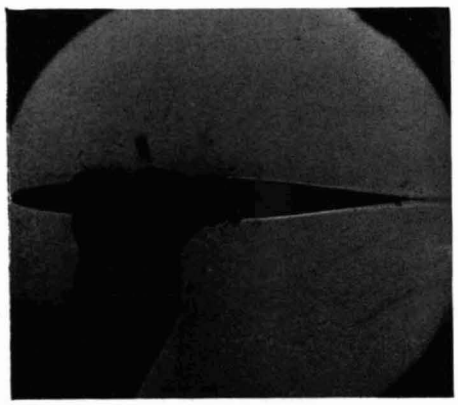

(a) $M = 0{\cdot}600$

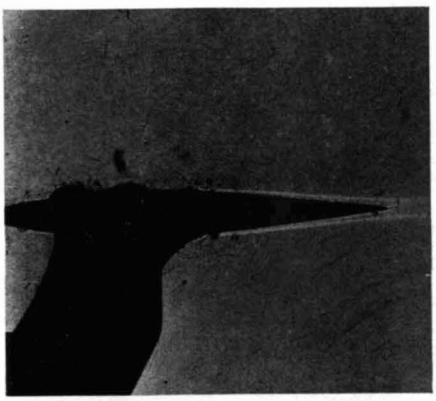

(b) $M = 0{\cdot}600$

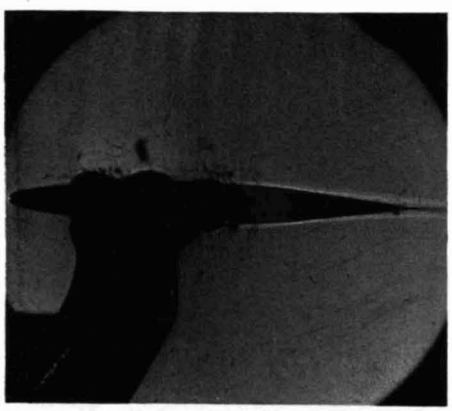

(c) $M = 0{\cdot}750$

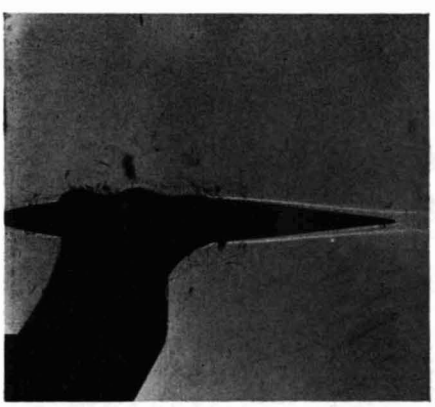

(d) $M = 0{\cdot}750$

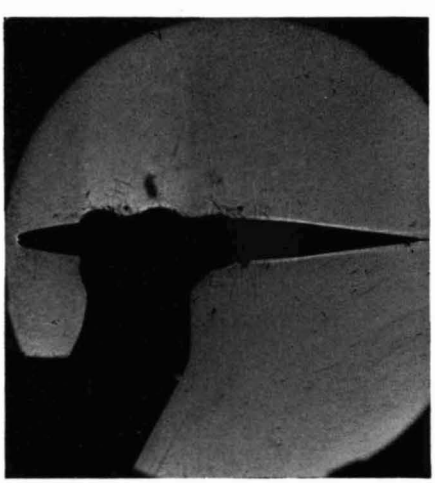

(e) $M = 0{\cdot}775$

FIG. 45. 10 per cent RAE 104 aerofoil. Direct-shadow photographs at $\alpha = 0$ deg.

Natural transition position

Fixed transition position
(Frigilene band at 0·14 chord on both surfaces)

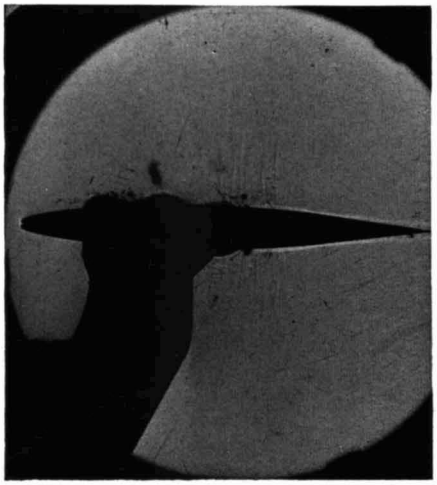

(f) $M = 0{\cdot}790$

Observed pressure $M_{crit} = 0{\cdot}785$

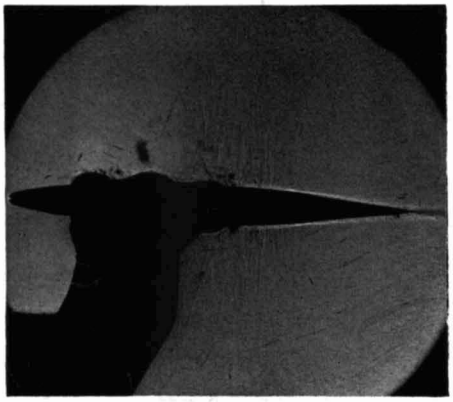

(g) $M = 0{\cdot}800$

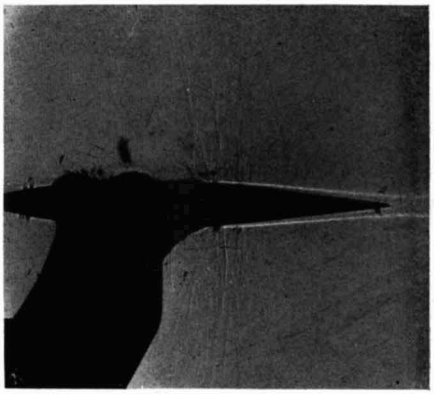

(h) $M = 0{\cdot}800$

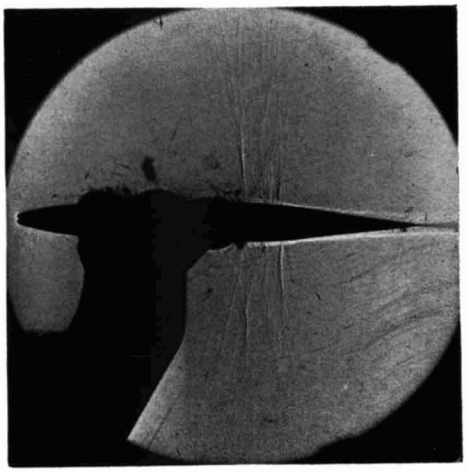

(i) $M = 0{\cdot}810$

FIG. 45—*continued.* 10 per cent RAE 104 aerofoil. Direct-shadow photographs at $\alpha = 0$ deg.

Natural transition position

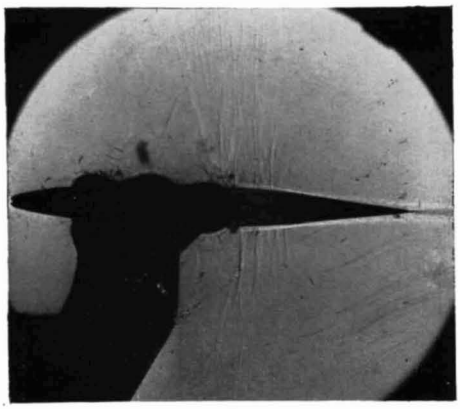

(j) $M = 0{\cdot}820$

Fixed transition position
(Frigilene band at 0·14 chord on both surfaces)

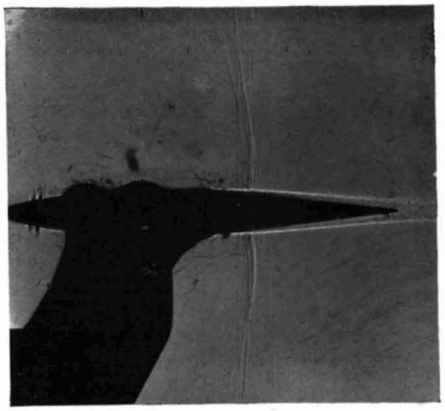

(k) $M = 0{\cdot}820$

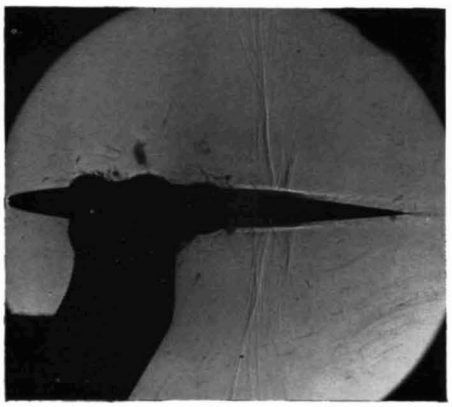

(l) $M = 0{\cdot}840$

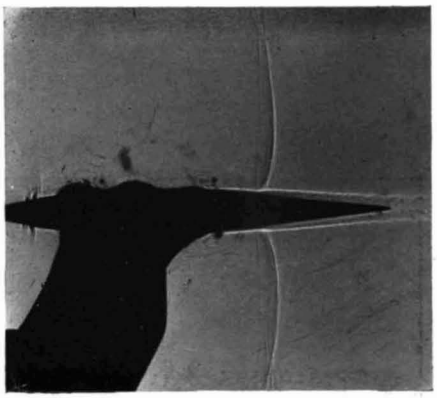

(m) $M = 0{\cdot}840$

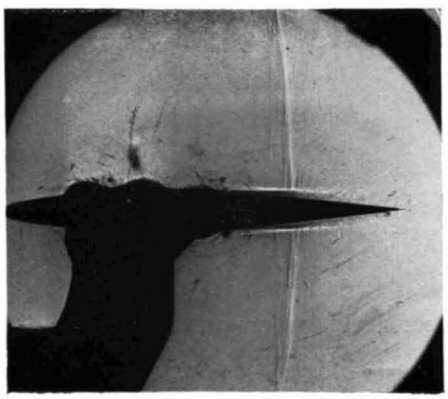

(n) $M = 0{\cdot}860$

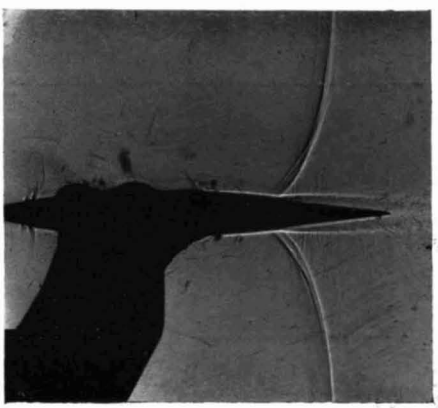

(o) $M = 0{\cdot}860$

FIG. 45—*continued.* 10 per cent RAE 104 aerofoil. Direct-shadow photographs at $\alpha = 0$ deg.

Natural transition position

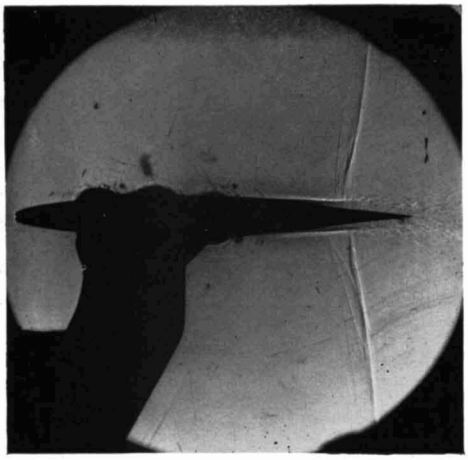

(p) $M = 0{\cdot}880$

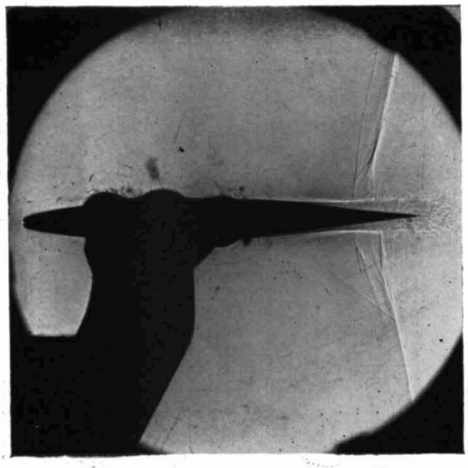

(q) $M = 0{\cdot}890$

FIG. 45—*continued.* 10 per cent RAE 104 aerofoil. Direct-shadow photographs at $\alpha = 0$ deg.

Natural transition position

Fixed transition position
(Frigilene band at 0·14 chord on both surfaces)

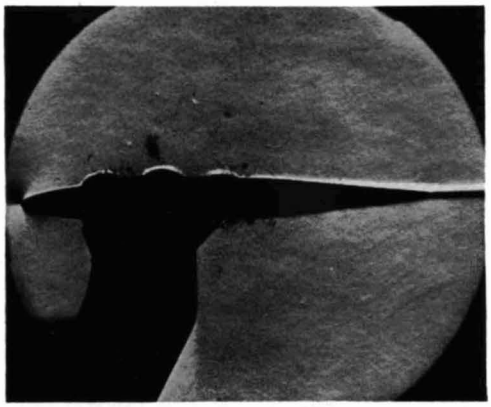

(a) $M = 0{\cdot}400$

Observed pressure $M_{crit} = 0{\cdot}785$

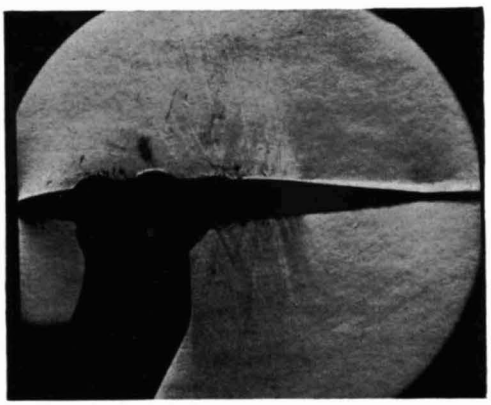

(b) $M = 0{\cdot}810$

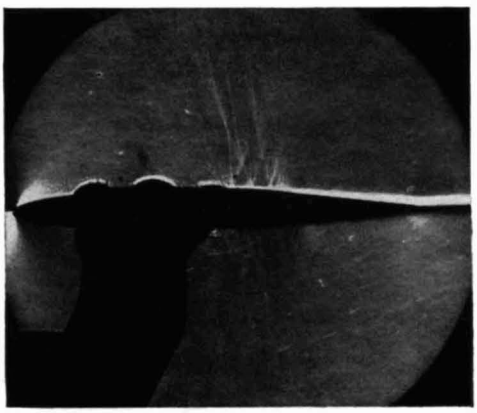

(c) $M = 0{\cdot}820$

(d) $M = 0{\cdot}820$

FIG. 46. 10 per cent RAE 104 aerofoil. Schlieren photographs at $\alpha = 0$ deg.

Natural transition position

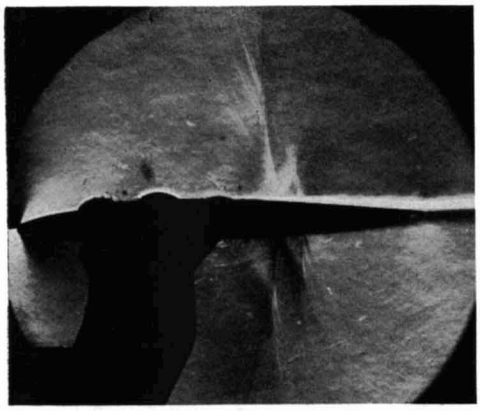

(e) $M = 0{\cdot}840$

Fixed transition position
(Frigilene band at 0·14 chord on both surfaces)

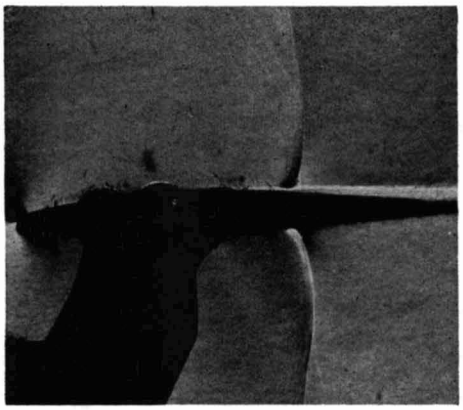

(f) $M = 0{\cdot}840$

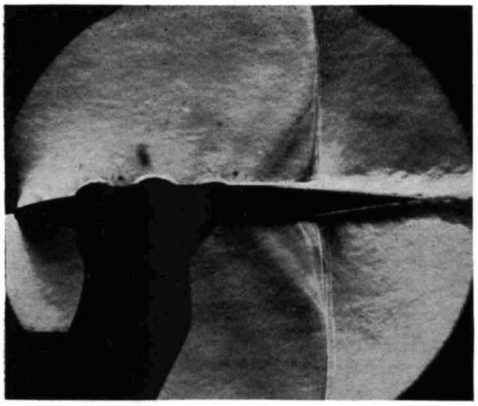

(g) $M = 0{\cdot}860$

(h) $M = 0{\cdot}860$

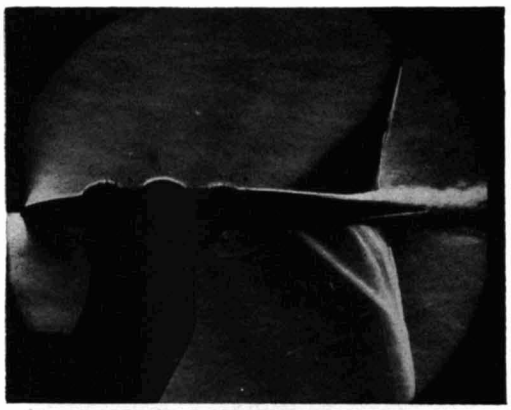

(i) $M = 0{\cdot}890$

FIG. 46—*continued.* 10 per cent RAE 104 aerofoil. Schlieren photographs at $\alpha = 0$ deg.

Natural transition position.

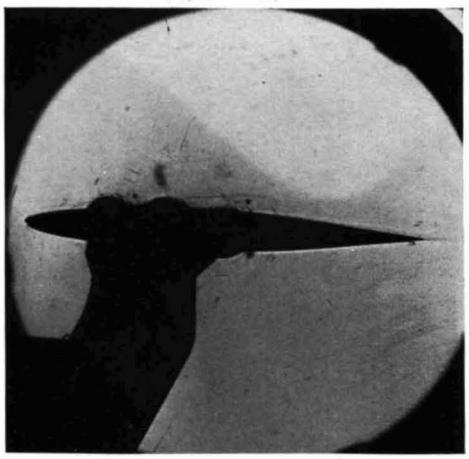

(a) $M = 0{\cdot}398$

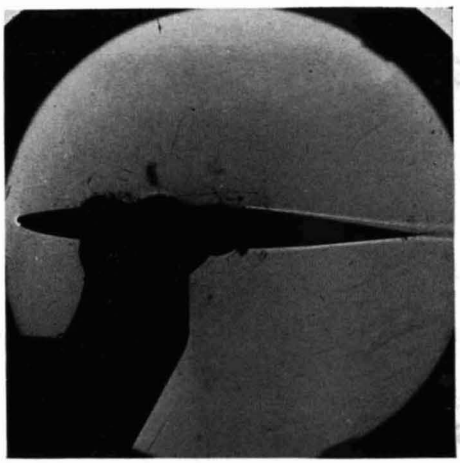

(b) $M = 0{\cdot}699$

Observed pressure $M_{crit} = 0{\cdot}720$.

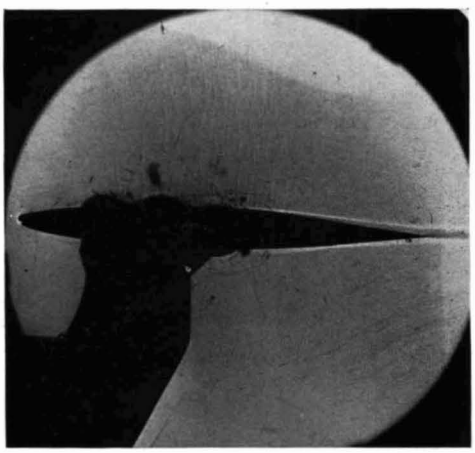

(c) $M = 0{\cdot}774$

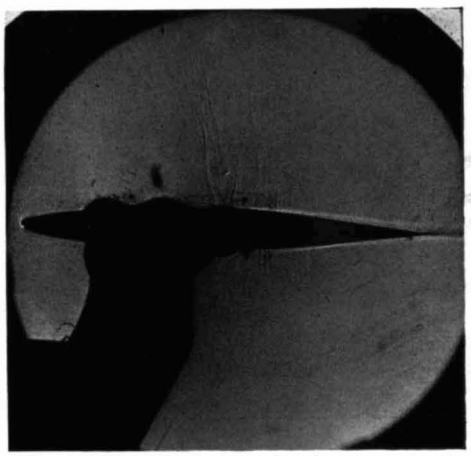

(d) $M = 0{\cdot}809$

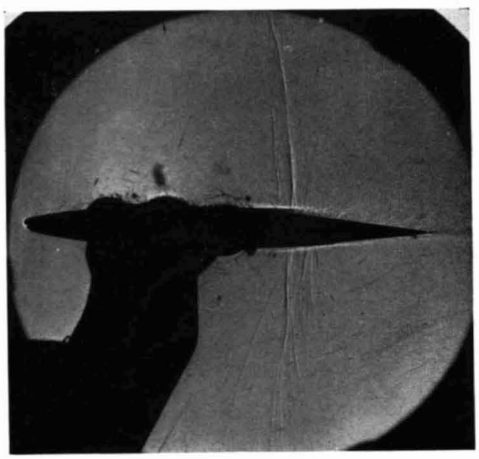

(e) $M = 0{\cdot}841$

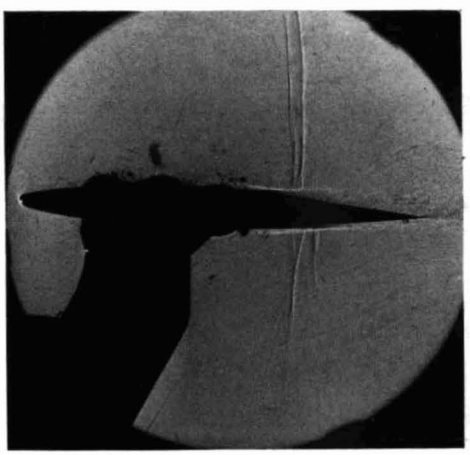

(f) $M = 0{\cdot}852$

FIG. 47. 10 per cent RAE 104 aerofoil. Direct-shadow photographs at $\alpha = 2$ deg.

Natural transition position

Fixed transition position
(Frigilene band at 0·14 chord on both surfaces)

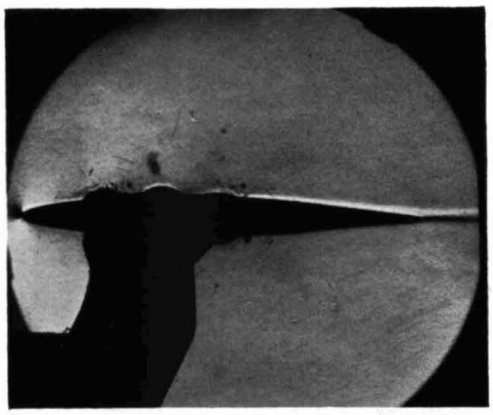

(a) $M = 0{\cdot}398$

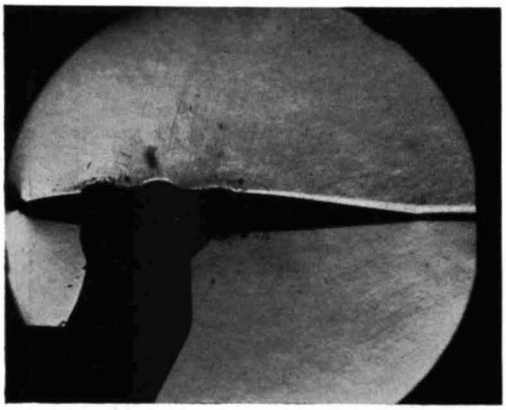

(b) $M = 0{\cdot}749$

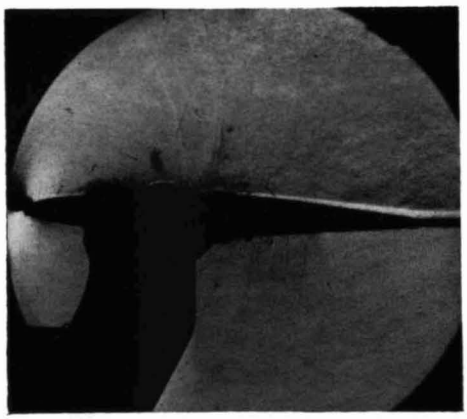

(c) $M = 0{\cdot}799$

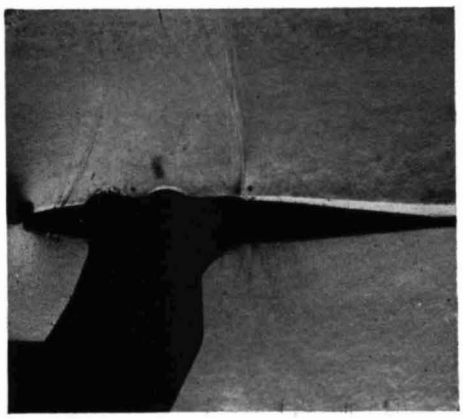

(d) $M = 0{\cdot}796$

FIG. 48. 10 per cent RAE 104 aerofoil. Schlieren photographs at $\alpha = 2$ deg.

Natural transition position

Fixed transition position
(Frigilene band at 0·14 chord on both surfaces)

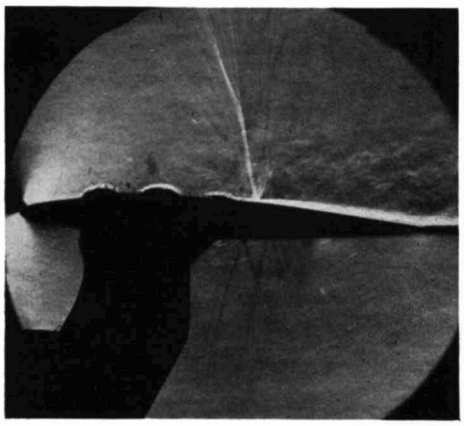

(e) $M = 0{\cdot}819$

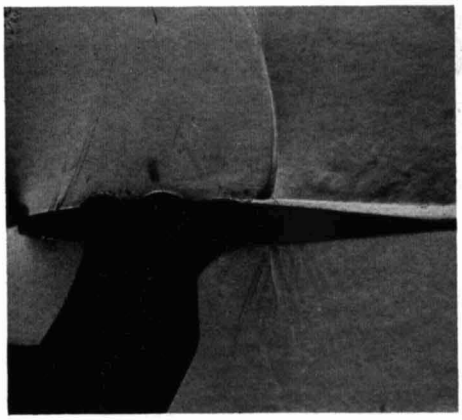

(f) $M = 0{\cdot}818$

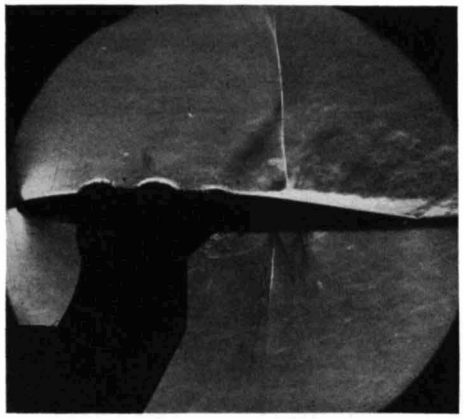

(g) $M = 0{\cdot}841$

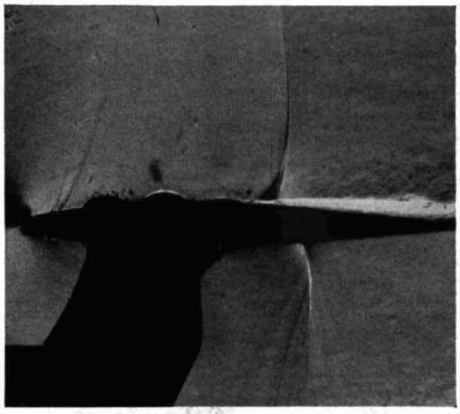

(h) $M = 0{\cdot}840$

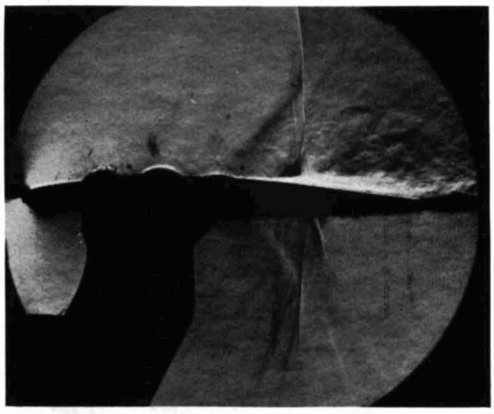

(i) $M = 0{\cdot}852$

FIG. 48—*continued.* 10 per cent. RAE 104 aerofoil. Schlieren photographs at $\alpha = 2$ deg.

Natural transition position

Fixed transition position
(Frigilene band at 0·14 chord on both surfaces)

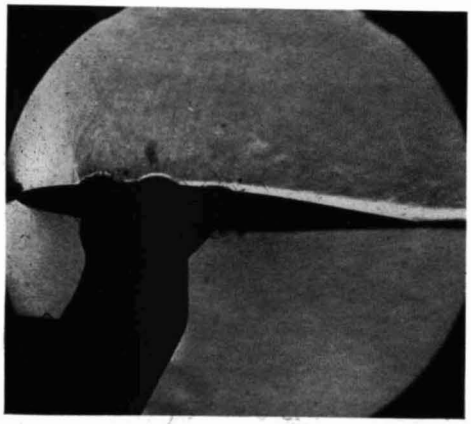

(a) $M = 0{\cdot}685$

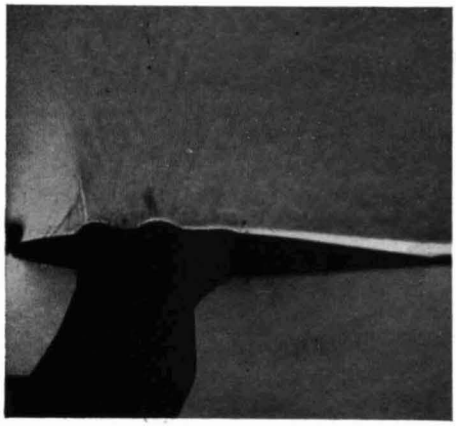

(b) $M = 0{\cdot}689$

Observed pressure $M_{crit} = 0{\cdot}550$

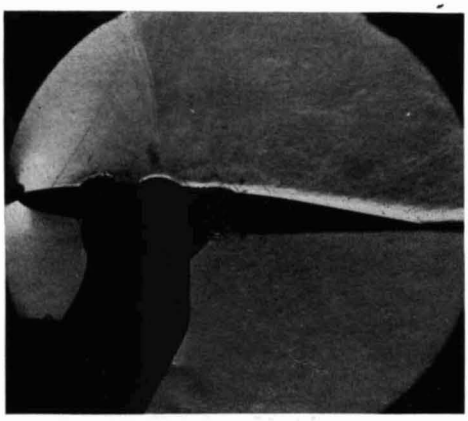

(c) $M = 0{\cdot}737$

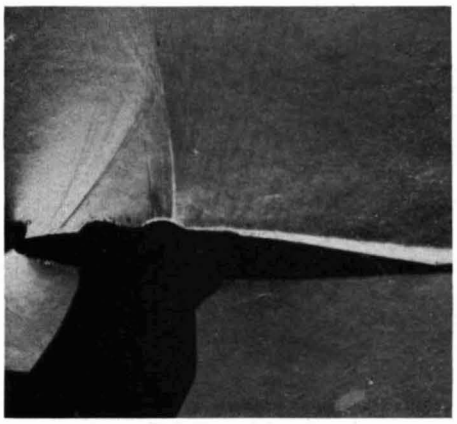

(d) $M = 0{\cdot}746$

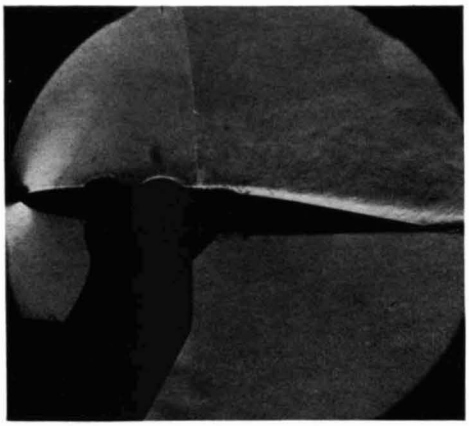

(e) $M = 0{\cdot}763$

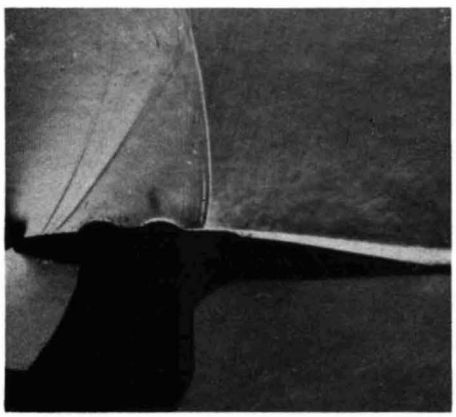

(f) $M = 0{\cdot}770$

FIG. 49. 10 per cent RAE 104 aerofoil. Schlieren photographs at $\alpha = 4$ deg.

Natural transition position

Fixed transition position
(Frigilene band at 0·14 chord on both surfaces)

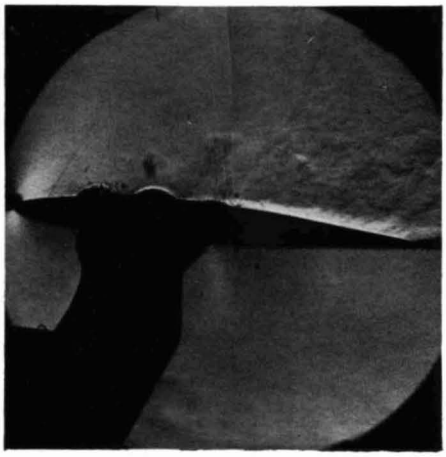

(g) $M = 0{\cdot}795$

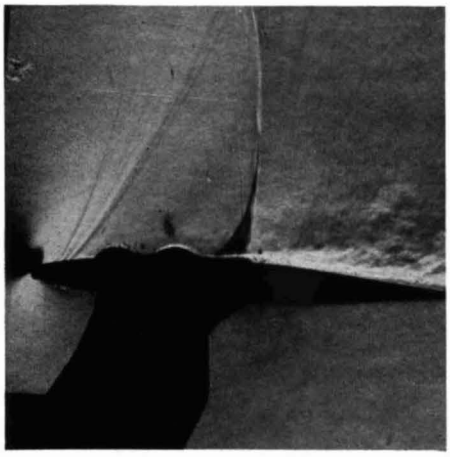

(h) $M = 0{\cdot}797$

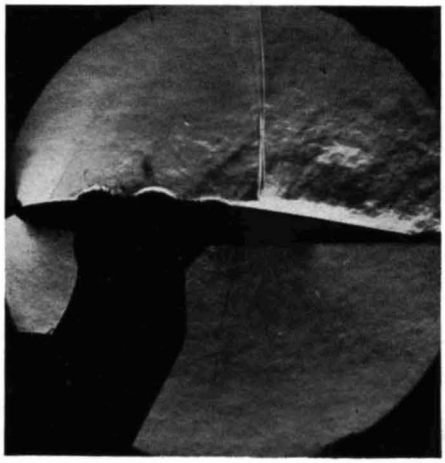

(i) $M = 0{\cdot}815$

(j) $M = 0{\cdot}814$

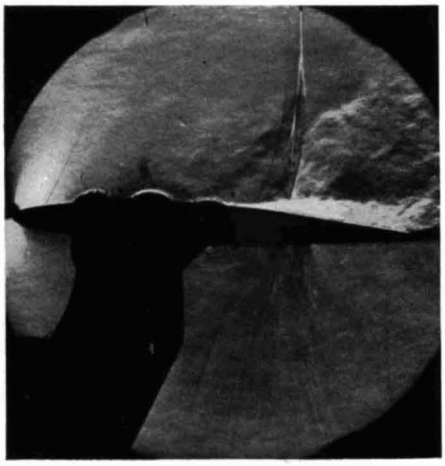

(k) $M = 0{\cdot}838$

(l) $M = 0{\cdot}835$

FIG. 49—*continued.* 10 per cent RAE 104 aerofoil. Schlieren photographs at $\alpha = 4$ deg.

Natural transition position.

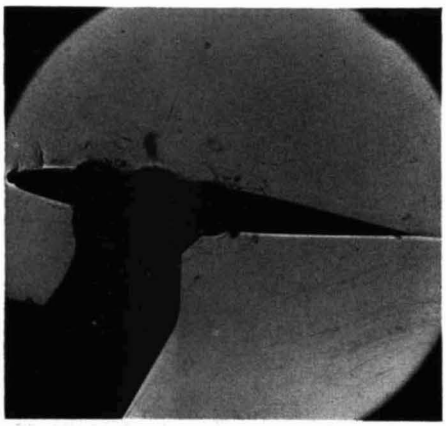

(a) $M = 0{\cdot}594$

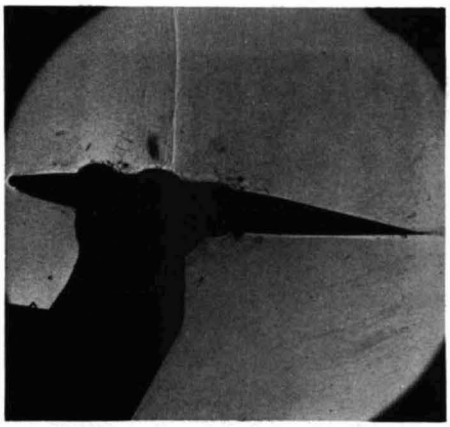

(b) $M = 0{\cdot}722$

Observed pressure $M_{crit} = 0{\cdot}530$

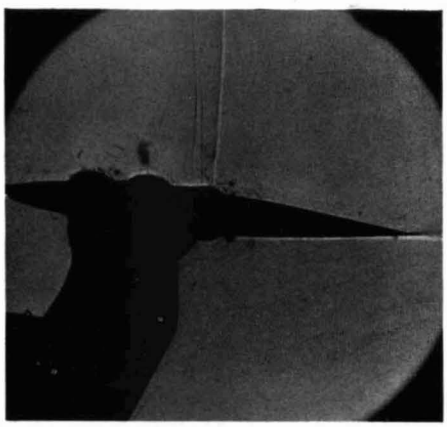

(c) $M = 0{\cdot}797$

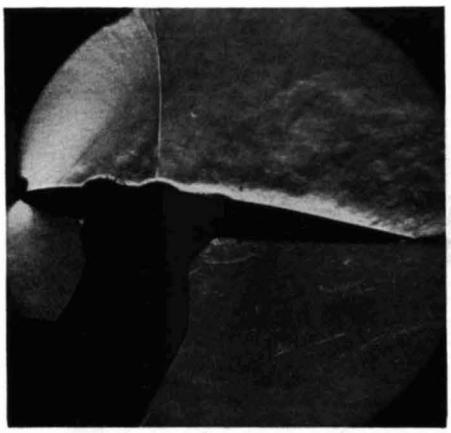

(d) $M = 0{\cdot}722$

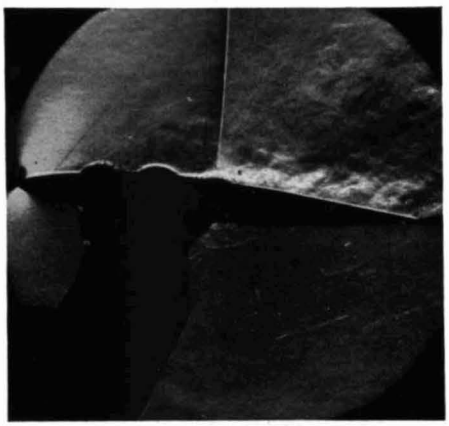

(e) $M = 0{\cdot}797$

(f) $M = 0{\cdot}820$

FIG. 50. 10 per cent RAE 104 aerofoil. Direct-shadow and Schlieren photographs at $\alpha = 6$ deg.

Natural transition position.

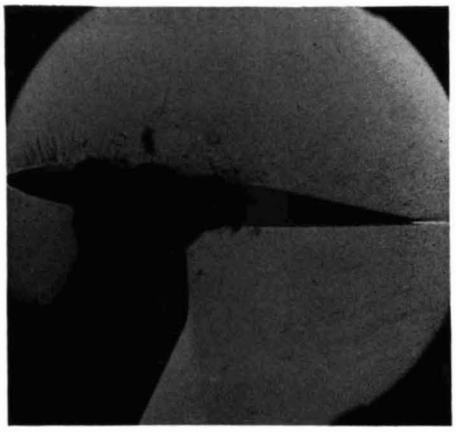

(a) $M = 0{\cdot}591$

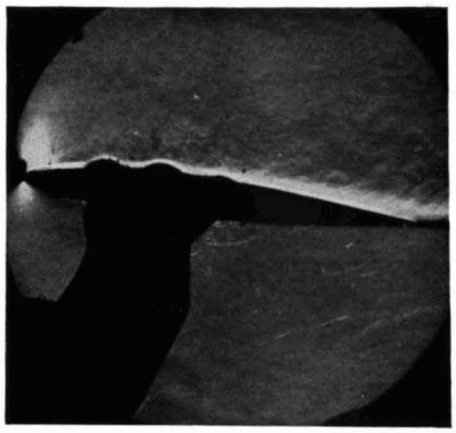

(b) $M = 0{\cdot}591$

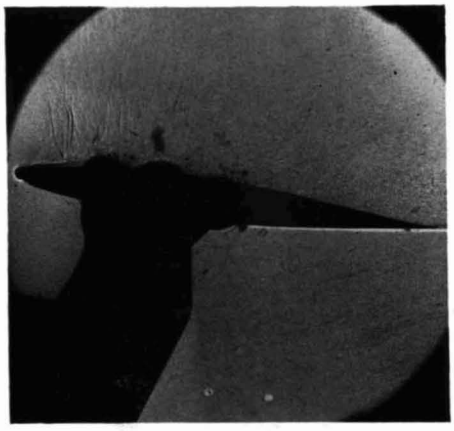

(c) $M = 0{\cdot}640$

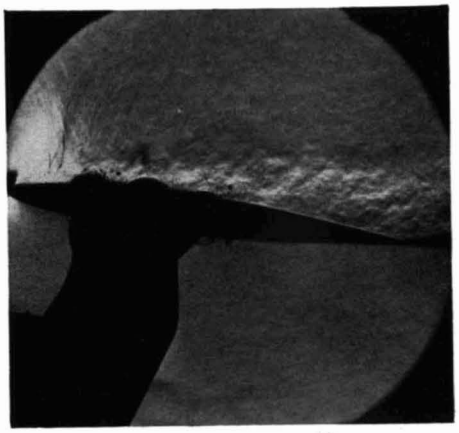

(d) $M = 0{\cdot}640$

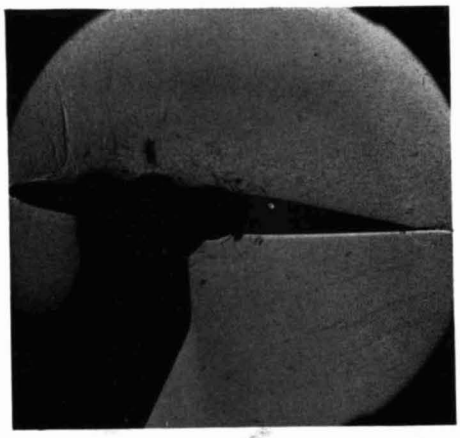

(e) $M = 0{\cdot}665$

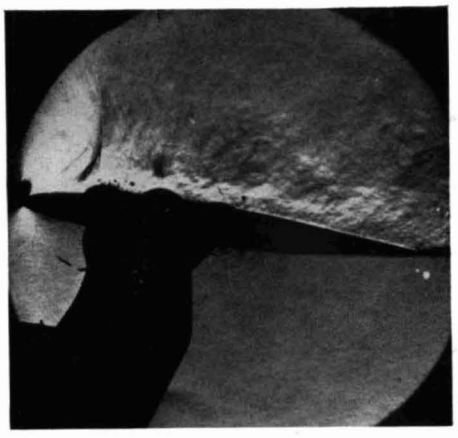

(f) $M = 0{\cdot}665$

FIG. 51. RAE 104 aerofoil. Direct-shadow and Schlieren photographs at $\alpha = 8$ deg.

(1522) Wt. 18/9296 K7 11/56 Hw.

PRINTED IN GREAT BRITAIN

Publications of the Aeronautical Research Council

ANNUAL TECHNICAL REPORTS OF THE AERONAUTICAL RESEARCH COUNCIL (BOUND VOLUMES)

1939 Vol. I. Aerodynamics General, Performance, Airscrews, Engines. 50*s.* (51*s.* 9*d.*).
Vol. II. Stability and Control, Flutter and Vibration, Instruments, Structures, Seaplanes, etc. 63*s.* (64*s.* 9*d.*)

1940 Aero and Hydrodynamics, Aerofoils, Airscrews, Engines, Flutter, Icing, Stability and Control Structures, and a miscellaneous section. 50*s.* (51*s.* 9*d.*)

1941 Aero and Hydrodynamics, Aerofoils, Airscrews, Engines, Flutter, Stability and Control Structures. 63*s.* (64*s.* 9*d.*)

1942 Vol. I. Aero and Hydrodynamics, Aerofoils, Airscrews, Engines. 75*s.* (76*s.* 9*d.*)
Vol. II. Noise, Parachutes, Stability and Control, Structures, Vibration, Wind Tunnels. 47*s.* 6*d.* (49*s.* 3*d.*)

1943 Vol. I. Aerodynamics, Aerofoils, Airscrews. 80*s.* (81*s.* 9*d.*)
Vol. II. Engines, Flutter, Materials, Parachutes, Performance, Stability and Control, Structures. 90*s.* (92*s.* 6*d.*)

1944 Vol. I. Aero and Hydrodynamics, Aerofoils, Aircraft, Airscrews, Controls. 84*s.* (86*s.* 3*d.*)
Vol. II. Flutter and Vibration, Materials, Miscellaneous, Navigation, Parachutes, Performance, Plates and Panels, Stability, Structures, Test Equipment, Wind Tunnels. 84*s.* (86*s.* 3*d.*)

1945 Vol. I. Aero and Hydrodynamics, Aerofoils. 130*s.* (132*s.* 6*d.*)
Vol. II. Aircraft, Airscrews, Controls. 130*s.* (132*s.* 6*d.*)
Vol. III. Flutter and Vibration, Instruments, Miscellaneous, Parachutes, Plates and Panels, Propulsion. 130*s.* (132*s.* 3*d.*)
Vol. IV. Stability, Structures, Wind Tunnels, Wind Tunnel Technique. 130*s.* (132*s.* 3*d.*)

Annual Reports of the Aeronautical Research Council—

1937 2*s.* (2*s.* 2*d.*) 1938 1*s.* 6*d.* (1*s.* 8*d.*) 1939–48 3*s.* (3*s.* 3*d.*)

Index to all Reports and Memoranda published in the Annual Technical Reports, and separately—

April, 1950 - - - - R. & M. 2600 2*s.* 6*d.* (2*s.* 8*d.*)

Author Index to all Reports and Memoranda of the Aeronautical Research Council—

1909—January, 1954 R. & M. No. 2570 15*s.* (15*s.* 6*d.*)

Indexes to the Technical Reports of the Aeronautical Research Council—

December 1, 1936—June 30, 1939	R. & M. No. 1850	1*s.* 3*d.* (1*s.* 5*d.*)
July 1, 1939—June 30, 1945	R. & M. No. 1950	1*s.* (1*s.* 2*d.*)
July 1, 1945—June 30, 1946	R. & M. No. 2050	1*s.* (1*s.* 2*d.*)
July 1, 1946—December 31, 1946	R. & M. No. 2150	1*s.* 3*d.* (1*s.* 5*d.*)
January 1, 1947—June 30, 1947	R. & M. No. 2250	1*s.* 3*d.* (1*s.* 5*d.*)

Published Reports and Memoranda of the Aeronautical Research Council—

Between Nos. 2251–2349	R. & M. No. 2350	1*s.* 9*d.* (1*s.* 11*d.*)
Between Nos. 2351–2449	R. & M. No. 2450	2*s.* (2*s.* 2*d.*)
Between Nos. 2451–2549	R. & M. No. 2550	2*s.* 6*d.* (2*s.* 8*d.*)
Between Nos. 2551–2649	R. & M. No. 2650	2*s.* 6*d.* (2*s.* 8*d.*)

Prices in brackets include postage

HER MAJESTY'S STATIONERY OFFICE

York House, Kingsway, London W.C.2; 423 Oxford Street, London W.1 (Post Orders: P.O. Box 569, London S.E.1)
13a Castle Street, Edinburgh 2; 39 King Street, Manchester 2; 2 Edmund Street, Birmingham 3; 109 St. Mary Street, Cardiff; Tower Lane, Bristol, 1; 80 Chichester Street, Belfast, *or through any bookseller.*

S.O. Code No. 23–2863